Designing Metal-Chelator like Traps by Encoding Amino Acids in Zirconium-based Metal-Organic Frameworks

Ainara Valverde,[1,2] Gabriel I. Tovar Jiménez,[3,4] Natalia A. Rio-López,[1] Dimas Torres,[3,4] Maibelin Rosales,[5] Stefan Wuttke, [1,6,] Arkaitz Fidalgo-Marijuan,[1] José María Porro,[1,6] Mónica Jiménez-Ruiz,[7] Victoria García Sakai,[8] Andreina García,[5,9] José Manuel Laza,[2] José Luis Vilas-Vilela,[1,2] Luis Lezama,[10] María I. Arriortua,[11] Guillermo Copello,[3,4] and Roberto Fernández de Luis[1,*]*

[1] Basque Center for Materials, Applications & Nanostructures (BCMaterials), Bldg. Martina Casiano, 3rd. Floor, Barrio Sarriena s/n, 48940, Leioa, Spain

[2]Macromolecular Chemistry Group (LABQUIMAC), Department of Physical Chemistry, Faculty of Science and Technology, University of the Basque Country (UPV/EHU), Barrio Sarriena s/n 48940 Leioa, Spain

[3]Facultad de Farmacia y Bioquímica. Departamento de Ciencias Químicas. Universidad de Buenos Aires. Buenos Aires, Argentina

[4]Instituto de Química y Metabolismo del Fármaco (IQUIMEFA). CONICET - Universidad de Buenos Aires. Buenos Aires, Argentina

[5]Advanced Mining Technology Center (AMTC), Universidad de Chile, Beauchef 850, Santiago, Chile.

[6]IKERBASQUE, Basque Foundation for Science, 48009 Bilbao, Spain

[7]Institut Laue Langevin, 71 Avenue des Martyrs, CS 20156, 38042 Grenoble, France

[8]ISIS Neutron and Muon Facility, Science & Technology Facilities Council, Rutherford Appleton Laboratory, Didcot, United Kingdom

[9]Mining Engineering Department, FCFM, Universidad de Chile, Av. Tupper 2069, 8370451 Santiago, Chile

[10]Dept. of Inorganic Chemistry, Science and Technology Faculty, University of the Basque Country (UPV/EHU), Barrio Sarriena s/n 48940 Leioa, Spain

[11]Dept. of Mineralogy and Petrology, Science and Technology Faculty, University of the Basque Country (UPV/EHU), Barrio Sarriena s/n, 48940, Leioa, Spain

KEYWORDS: Metal-organic frameworks, MOFs, Amino acids, Selective Adsorption, Metalation, Heavy metal capture.

ABSTRACT

Metal chelators and porous sorbents are two of the forefront technologies applied for the recovery and separation of hazardous and/or valuable metal ions from aqueous solutions. (*i.e.* polluted water sources, metal-rich mining wastewaters, acid leachates…). The transfer of the metal coordination functions of metal-chelators to chemically stable host materials had so far only limited success. Here, we report the installation of natural acids (*i.e.* malic acid, mercaptosuccinic acid, succinic acid, fumaric acid and citric acid) and amino acids (*i.e.* histidine, cysteine and asparagine) within a porous zirconium-based trimesate metal-organic framework (MOF), namely MOF-808. Applying this strategy, we were able to produce a pore environment spatially decorated with multiple functional groups usually found in commercial chelator molecules. The chemical stability of the amino acid molecules installed by solvent assisted ligand exchange has been studied to delimitate the applicability window of these materials. The adsorption affinity of MOF-808@(amino)acids in static and column-bed configurations can be fine-tuned as a function of the amino acid residues installed in the framework. MOF-808(Amino)acid columns can be applied efficiently both for water remediation of heavy metals, and for the separation of metal-ions with different acidities. For instance, the initial trends for the dispersion of rare earth elements have been identified. EPR and Inelastic Neutron Scattering spectroscopy reveals that MOF-808@(amino)acids stabilize metal centers as isolated and clustered species, in a coordination fashion that involves both the amine and thiol functions, and that affects the vibrational freedom of some of the chemical groups of the amino acid molecules. The metal-ions stabilization within an amino acid decorated MOFs opens the avenue to the application for pseudo bio-catalysis purposes in the near future.

INTRODUCTION

The selective adsorption of metal ions from aqueous solutions is a pivotal process for environmental remediation,[1] but it is also a technology of paramount importance for metal separation purposes. The recovery and purification of metal ions from polluted water sources are increasingly gaining importance within the concept of a closed loop circular economy.[2] For instance, the recovery and separation of critical raw materials from acid waters derived from mining activities,[3] rare-earth elements (REE) uptake from water streams arising from phosphor-gypsum deposits,[4] or the precious metals (*i.e.* palladium) recovery from radioactive wastewaters,[5–8] are some of the relevant application-areas where an intensive research is in place to develop a greener and more efficient capture and separation technologies. It is important to note, that each of these scenarios demands specific requirements, being chemical resistance, specificity of adsorption and continuous flow-operation capacity, three of the key figures of merit that weigh the technical applicability of the metal-separation technology.

Today, metal-chelating agents and adsorbents are the simplest, cost efficient and flexible (in terms of design/operation and regeneration) technologies applied for the metal-ions capture, separation and purification purposes.[9] On one hand, chelation is a type of bonding of chelating agents to metal ions that involves the formation of two or more separate coordinate bonds between a polydentate (multiple bonded) ligand and a single central metal atom.[10,11] The efficiency and selectivity of the chelation-based solvent extraction of a metal depends on the coordination chemistry behind the process and the chemical structure of the chelator itself.[12,13] Although engineering of these polydentate molecules has great flexibility, solvent extraction makes the recovery of the metal-chelator complexes time and energy consuming, and even environmentally

unfriendly for specific applications. On the other hand, adsorption has attracted considerable attention due to its simplicity and cost efficiency.[14] Classic sorbents as zeolites[15], clays[16] or activated carbons[17], although easier to recover and reactivate than soluble metal-chelators, suffer from low adsorption capacity[18] and selectivity due to their limited chemical tailorability.

Among the multiple approaches to replicate the metal binding modes of organic chelators in solid porous materials, the chemical encoding of a particular class of porous ordered materials called Metal-organic frameworks (MOFs) holds enormous promise.[19–22] MOFs are crystalline solids built from metal ions or clusters connected by organic linkers into extended, ordered, and highly porous networks.[23–31] Thanks to their impressive porosity metrics (*i.e.* large surface area, a big pore volume/window…), and their versatility to be encoded with specific functionalities, the MOFs have been successfully applied to capture or separate metal ions from different aqueous media (*i.e.* polluted freshwater, seawater or acid leachates).[32–35] Solvent assisted ligand exchange (SALE) or postsynthetic exchange (PSE) functionalization of zirconium MOFs is one of the most facile and versatile experimental protocols to anchor metal-chelating motifs into the defective positions of these materials.[36–40] For example, the chemical versatility of the zirconium trimesate (MOF-808), together with its mesoporous structure, has opened the perspective to an easy installation of small to bulky functionalities, while preserving long range order of the backbone structure. Just as a relevant example, Y. Peng *et al.*[14] have successfully installed the well-known ethylenediaminetetraacetic acid (EDTA) chelator into the MOF-808 structure endowing the material of impressive adsorption capacity towards a broad scope of metal-ions with varied acidities. Even though MOF-808@EDTA lacks strong selectivity over the capture of a specific ion, the adsorption experiments performed in a continuous flow with a multielement solution pointed that the breakthrough volume of the MOF-808@EDTA column was dependent on the

metal acidity, suggesting that alternative encodings of the pore space of the MOF-808 may lead to a stronger column breakthrough dispersion of the metal-ions.

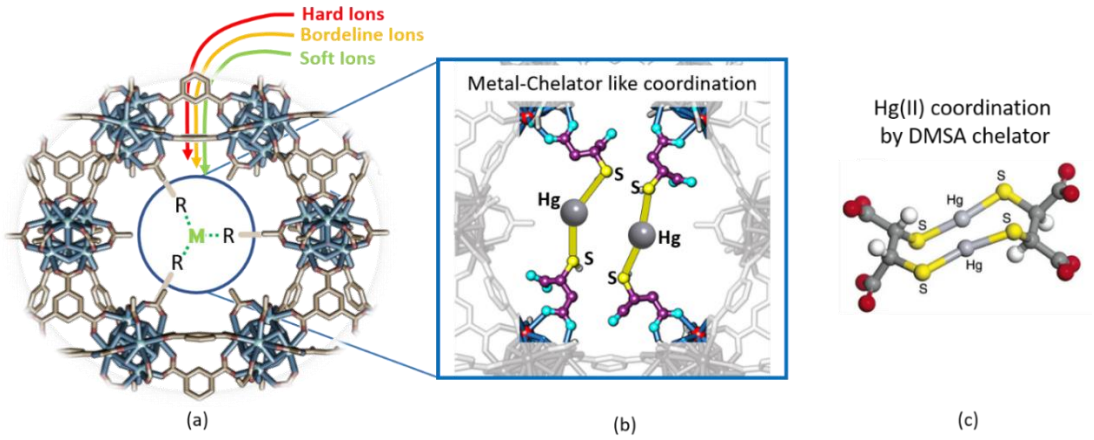

Figure 1. (a) Illustration of hard, borderline and soft metal-chelator like traps within the MOF-808 scaffold. (b) Illustration of the a tentative placement of the mercaptosuccinic molecules into the MOF-808 pore space and their coordination to Hg(II). (c) Coordination modes of dimercaptosuccinic acid (DMSA) chelators over Hg(II) ions.

As a general rule, the density and the hard/soft nature of the metal binding functions encoded in the MOFs' pores, determine their metal ion adsorption capacity and affinity.[7,41–44] Thus, in this work we have explored the pore space functionalization of MOF-808 scaffold with amino acids (*i.e.* histidine, cysteine and asparagine) and natural acids (*i.e.* malic acid, mercaptosuccinic acid, succinic acid, fumaric acid and citric acid) having residual groups of different natures in order to fine-tune the metal-ion adsorption specificity of the parent MOF-808 material.[41,45] The chemical structure and the molecular size of the amino acids and natural acids functions have been selected in order to engineer a MOF-808 pore space able to act as a multidentate chelator for metal ions.

The chemical stability of the functionalities installed by solvent assisted ligand exchange has been assessed simulating the acidity and anion strength conditions that could be found in natural waters (*i.e. arsenic polluted water of the north of Chile*),[46] acid waters (*i.e. waste water coming from mining or industrial activities*),[47] and water media with high anionic strengths (*i.e. acid-waters from phosphor-gypsum deposits*)[4]. Finally, the specificity of adsorption has been tested in batch and continuous flow conditions in single and multielement solutions. The metal-binding modes of the most promising MOF-808@cysteine variant have been identified by a combination of electron paramagnetic resonance and inelastic neutron spectroscopies.

MATERIALS AND METHODS

Synthesis and post-synthetic functionalization of MOF-808

H_3BTC (2.1 g, 10 mmol) and $ZrOCl_2 \cdot 8H_2O$ (9.7 g, 30 mmol) were dissolved in two dimethylformamide (DMF)/formic acid solutions (225 mL/225 mL each) and mixed in a 1-L screw-capped glass jar. Afterwards, the reaction was performed at 130 °C for 48 h in an isothermal oven.[48] The white precipitate was collected by centrifugation and washed 4 times with DMF (100 mL x2) and MeOH (100 mL x2) over a period of 24 h. The sample was then activated at 80 °C for 24 h and stored at room conditions into a sealed vial.

Solvent assisted formate anion exchange (SALE)[49–51] was performed with water solutions of eight natural acids and amino acids: a) L-asparagine (Asp), b) L-histidine, (His) c) mercaptosuccinic acid (Msc), d) L-cysteine (Cys), e) succinic acid (Suc), f) fumaric acid (Fum), g) L-malic acid (Mal), and h) citric acid (Cit). Starting with L-cysteine, we screened the concentration of the

SALE solution (0.15, 0.10 and 0.05 M) at a temperature of 60 ºC monitoring the crystallinity of the XRD patterns and the trimesic acid (BTC) - cysteine molar ratio in the compounds by ^{1}H-NMR after the functionalization. We selected the following optimized conditions to achieve the higher functionalization degree as possible while maintaining the crystallinity of the MOF-808 after the SALE. A more detailed information about the post-synthetic functionalization protocol is described in the main results and discussion section.

Optimized conditions for (amino)acid functionalization of MOF-808: 300 mL of 0.05 M water solutions of the amino(acids) were prepared in a 500 mL autoclave at 60 °C. MOF-808 (600 mg) was dispersed under continuous stirring during 1h in the (amino)acid solution and heated at 60 °C for 24 h in an isothermal oven. MOF-808@(amino)acid was recovered by centrifugation (x6500 rpm), washed 3 times with 100 mL water (24 h each) and then with 100 mL methanol other 3 times (24 h each). Finally, the samples were dried at 80 °C overnight (12 h) and stored in a desiccator.

MOF-808 general characterization protocols

MOF-808@(amino)acids were characterized by X-ray diffraction, infrared spectroscopy, thermogravimetry and N_2 sorption at 77 K. A detailed description of the sample preparation, data curation and analysis can be found in the supplementary material (section 1 in the SI). The presence and quantification of the (amino)acid functionalities was performed by ^{1}H-NMR spectroscopy. To this end, 20 mg of the samples were digested in 0.7 mL of NaOH deuterated solution (1 M) overnight. The mixture was centrifugated at 7000 rpm. The solution was recovered carefully with a syringe, preventing the uptake of powdered material settled at the bottom of the centrifuge tube. The experiments were performed on a Bruker AV500 equipped with a BBI probe and Z-axis gradients, operating at a frequency of 500 MHz for proton and 125.77 MHz for carbon. Data acquisition and processing was carried out with TOPSPIN 2.1 software (Bruker). The pulse

sequences used were the Bruker standard. Once the H^1-NMR spectra were acquired, the (amino)acid content per formula unit was calculated by integrating the signals associated to the (amino)acids, and fingerprint peak (8.26 ppm) associated to the trimesic acid molecules. The MOF functionalization and the posterior ^{1}H-NMR quantification of the trimesic:(amino)acid molar ratio has been done by triplicate in order to evaluate the accuracy that can be achieved by replicating the experimental protocol. Chemical formulas for each MOF-808@(amino)acid sample have been summarized in the Table 1. As described in detail in the results and discussion section, 0.08 linker defects per formula unit have been calculated for the parent MOF-808 material by the analysis of the last weight loss of the TGA curve. The strong overlapping of the thermal release of the (amino)acid functions and the trimesic acid calcination observed in the TGA measurements of MOF-808@(amino)acid samples, hinders elucidating if additional trimesic linker defects have been generated during the (amino)acids incorporation to the porous framework of MOF-808. We have assumed that the trimesate defects in MOF-808@(amino)acid samples is close to the one calculates for the parent MOF-808 material, although some degree of linker displacement by (amino)acid molecules could occur during SALE. The charge neutrality of the chemical formulas was achieved by balancing the (amino)acid and formate content on the basis of the data obtained from ^{1}H-NMR, and balancing the additional positive unbalanced charges arising from linker defective sites in the clusters, with one hydroxyl and one water molecule per position. For di-topic or tri-topic carboxylates as fumaric, succinic, malic, mercaptosuccinic and citric acids we have assumed that the carboxyl groups not coordinated to the clusters are protonated.

Table 1.- Chemical formula for MOF-808@(amino)acid samples.

	Formula	Cluster:AA*
MOF-808	$Zr_6O_4(OH)_{6.58}(H_2O)_{2.58}(C_9O_6H_3)_{1.92}(HCOO)_{3.5}$	--
Asp	$Zr_6O_4(OH)_{7.19}(H_2O)_{2.19}(C_9O_6H_3)_{1.92}(HCOO)_{1.25}(C_4H_7N_2O_3)_{3.40}$	1:3.4(4)
His	$Zr_6O_4(OH)_{4.44}(H_2O)_{0.44}(C_9O_6H_3)_{1.92}(HCOO)_{0.8}(C_6H_8N_3O_2)_{5.00}$	1:5.0(3)
Msc	$Zr_6O_{4.0}(OH)_{5.94}(H_2O)_{1.94}(C_9O_6H_3)_{1.92}(C_4H_5O_4S)_{4.30}$	1:4.3(4)
Cys	$Zr_6\ O_{4.0}(OH)_{5.89}(H_2O)_{1.89}(C_9O_6H_3)_{1.92}(HCOO)_{0.7}(C_3H_6NO_2S)_{3.65}$	1:3.7(2)
Suc	$Zr_6\ O_{4.0}(OH)_{6.79}(H_2O)_{2.79}(C_9O_6H_3)_{1.92}(C_4O_4H_4)_{3.45}$	1:3.5(3)
Fum	$Zr_6\ O_{4.0}(OH)_{6.74}(H_2O)_{2.74}(C_9O_6H_3)_{1.92}(C_4O_4H_2)_{3.36}$	1:3.4(2)
Mal	$Zr_6\ O_{4.0}(OH)_{5.64}(H_2O)_{1.64}(C_9O_6H_3)_{1.92}(HCOO)_{0.25}(C_4H_5O_5)_{4.60}$	1:4.6(4)
Cit	$Zr_6\ O_{4.0}(OH)_{7.06}(H_2O)_{3.06}(C_9O_6H_3)_{1.92}(HCOO)_{0.4}(C_6H_7O_7)_{2.78}$	1:2.8(4)

*AA= (amino)acid

MOF-808@(amino)acid chemical stability

The chemical stability of (amino)acid functionalities incorporated to the MOF-808 was assessed by immersing 100 mg MOF-808@(amino)acid in 100 mL water solutions with pH values of 4, 3 and 2. Afterwards, the samples were characterized by powder X-ray diffraction and ^{1}H-NMR spectroscopy in order to *i*) inspect if the long-range order of the crystal structure is maintained or altered in some degree, and *ii*) to quantify if the BTC : amino acid molar ratio varies in comparison to the one of the initial MOF-808@(amino)acid.

Metal-adsorption screening

The adsorption affinity of the MOF-808@(amino)acid frameworks over metal ions with varied acidities (i.e. Z^+/r^2) was determined performing adsorption tests in single metal aqueous solutions with a concentration of 100 ppm. MOF-808@(amino)acids (10 mg) were dispersed in 5 mL - 100

ppm water solutions of Hg(II), Pb(II), Cd(II), Cu(II), Ni(II), Eu(III), Y(III), La(III), Cr(III), and Cr(VI). Eu(III), Y(III), La(III), Pb(II) and Cd(II) solutions were prepared with nitrate salts; Hg(II), Ni(II) and Cr(III) solutions were prepared with chloride salts, and Cr(VI) solution was obtained from potassium dichromate salt. The dispersion was stirred overnight (12 h) under isothermal (21 °C) and dark conditions. After adsorption equilibrium was reached, the dispersion was centrifuged and filtered with a nylon syringe filter (Branchia, pore: 0.22 μm, diameter: 25 mm). Finally, 3 mL aliquots were taken, acidified with 100 μL of HNO_3 and measured after dilution to the proper metal concentration range with an ICP-AES Horiba Yobin Yvon Activa.[42,52,53] Adsorption capacity of MOF-808@(amino)acid samples was determined on the basis of Equation 1:

$$Q_e = (([M]_i - [M]_f)\cdot V)/m \qquad \text{Eq. 1.}$$

where $[M]_i$ and $[M]_f$ are the metal initial and final concentrations (mg/L), V is the volume of the solution (L) and m is the mass of adsorbent.

Competitive adsorption experiments

Competitive adsorption experiments were performed in a multielement solution of soft (Hg(II); Pb(II)), intermediate (Cd(II), Cu(II), Ni(II)) and hard metal ions (Eu(III), La(III), Y(III), Cr(III)), each of them in a concentration close to 10 ppms. Although the concentration of the metals in the multielement solutions applied in competitive adsorption experiments are usually tailored to the ones observed in the final scenarios of application (*i.e. recovery of REE from acid polluted waters, capture of Pd-ions from radioactive wastewater…*), we decided to use the same concentration for all the metals in order to confirm if the adsorption affinity observed in the metal adsorption

screening experiments is maintained in a complex mixtures containing multiple ions. The metal-ion adsorption selectivity was evaluated determining the distribution coefficient K_d for each metal, as described in the equation 2:

$$K_d = \frac{V}{m}\frac{(C_0 - C_e)}{C_e} \quad \text{Eq. 2}$$

where, V is the volume of the solution in mL, m is the mass of the adsorbent in grams and C_0 and C_e are the concentration of the metals in the solution at the initial and equilibrium points of the adsorption. The separation factor (SF) was calculated as described by the equation 3 to identify the MOF-808@(amino)acid sorbents that could be applied to separate ions from the multielement solutions with factors of at least above three between two different ions.

$$SF = \frac{K_d^A}{K_d^B} \quad \text{Eq. 3}$$

where K_d^A and K_d^B are the distribution factors for the metals A and B calculated for the same adsorbent material.

Continuous flow metal-ions separation with MOF-808@(amino)acid columns.

When designing continuous flux adsorption experiment, it is necessary to integrate the MOF in a highly permeable chromatographic column that at the same time maximizes the contact between the aqueous solution and the active MOF sorbent. First, the protocol described by Rapti *et al.*[54] was followed to assemble a MOF-808@(aminoacid)/sand (15% w/w : 150 mg of MOF dispersed in 1500 mg of sand) based chromatographic column. The mixture was homogenized and packed in a glass column of 0.25 cm inner diameter, and approximately 1.5 cm height. A peristaltic pump was used to control the flux of the multi-metal solution through the column at 0.5 mL per minute.

The multielement solution was prepared as described in the previous section. Aliquots from the output-solution where taken approximately each 60 min of the experiment, until the complete breakthrough of the column was achieved by most of the metals of the multielement solutions. The concentration of the metal in the input and output solutions were monitored by ICP-MS. Variance of the concentration of the metals was normalized taking into account their initial concentration.

The final data was fitted to the Thomas model described in the equation 4. The mathematical models such Thomas are used to describe a dynamic behavior of the pollutants capture in a fixed-bed column assuming negligible external and internal diffusion limitations.

$$\frac{C_t}{C_o} = \frac{1}{1+\exp\left[\frac{k_T}{Q}(q_o m - C_o t)\right]} \quad \text{Eq. 4}$$

where k_T is the Thomas rate constant ($L \cdot mg^{-1} \cdot min^{-1}$), C_0 is the initial metal concentration ($mg \cdot L^{-1}$), C_t is the equilibrium concentration at a given t (min), q_0 is the maximum column adsorption capacity ($mg \cdot g^{-1}$), Q is the volumetric flow rate ($L \cdot min^{-1}$) and m is the mass of the adsorbent in the column (g). From the fitting of the experimental data with the Thomas equation, the overall adsorption of the column and the Thomas constant (k_T) are usually obtained, as summarized in the Table S5.

Adsorption isotherms and kinetics: Adsorption isotherms were obtained for Pb(II), Cd(II) and Hg(II) using MOF-808@Cys and MOF-808@His samples. The experiments were conducted with 10 mg MOF-808@amino acid dispersed in 5 mL of metal solutions with different concentrations from 1 to 2000 ppm. The solutions were put under magnetic stirring overnight (12 h) until adsorption equilibrium was reached. After that, the suspension was removed with a hydrophilic 0.22 μm filter, it was acidified for its stabilization, and finally it was analyzed by means of ICP-

AES. Adsorption capacity for each point of the isotherm curve was determined on the basis of Equation 1. Adsorption isotherms were fitted to Langmuir and Freundlich models (section S3.1).[55–57]. Adsorption kinetics curves were obtained as well for Pb(II) and Hg(II). To this end, 10 mg of MOF-808@amino acid was dispersed in a 5 mL – 100 ppm water solution of the metal ion and further stirred under isothermal and dark conditions. The adsorption process was stopped at different time intervals (5 – 1400 min) by removing the MOF sorbent through centrifugation (6500 rpm, 3 min). The solution was further filtrated with a hydrophilic 0.20 μm filter, acidified with 100 μL 0.1 M HNO_3, and analyzed by ICP-AES after its dilution (if necessary). Bangham model was applied to fit the experimental data (section S3.2).[2,58]

The metal adsorption efficiencies of MOF-808@(amino)acid samples for Hg(II), Pb(II), and Cd(II) were evaluated in metal concentrations ranges close to these ones found in polluted water sources (1 ppm). In this experiment, the initial and final metal concentrations of the heavy metals were determined with an ICP-MS Agilent 7700 spectrometer.

Inelastic Neutron Scattering and Electron paramagnetic resonance spectroscopic for the characterization of the adsorption sites

The Inelastic Neutron Scattering (INS) spectra were measured at 10 K in the range of energy transfers from 160 to 2000 cm^{-1} (that corresponds to 20-250 meV) with an energy resolution of $\Delta E/ \Delta E \sim 2$ % using the IN1-Lagrange neutron spectrometer installed at the hot source of the high-flux reactor at the Institut Laue-Langevin in Grenoble.[1,2]. The energy transfer was calculated by subtracting 4.5 meV, the constant final energy of the PG analyzers, from the energy of the incoming neutrons selected with a focusing Cu(220) single crystal. The background spectrum from

the cryostat and an empty sample holder was measured separately and then subtracted from the raw INS spectrum of the sample. In the extent that k_f is much smaller than k_i (and therefore high Q), the observed intensity is directly proportional to the generalized density of states (GDOS), that is the hydrogen partial density of states in the case of hydrogenated materials. Data sets were then normalized for monitor counts and corrected for empty cells. The calculated relative intensity of the th mode determined at a momentum transfer Q and at an energy transfer, S, of an INS band is given by [3]

$$S(Q, n\,\omega_\nu) \sim ((Q\,{}^{\nu}u_l)^{2n})/n!\,\exp[-(Qu_{Tot})^2]\sigma_l \qquad \text{Eq. 5}$$

where ω_ν is the n^{th} mode at frequency ω n=1 for a fundamental, 2 for a first overtone or binary combination, 3 for a second overtone or ternary combination, etc., **Q** is the momentum transfer, ${}^{n}u_l$ is the atomic displacement of the atom *l* in the mode, u_{Tot} is the root-mean-square displacement of all atoms in all the modes and $\sigma_{l\,l}$ is the scattering cross section of the atom *l*. The exponential term in Eq. 3 is the Debye-Waller factor and its magnitude is in part determined by the thermal motion of the molecule. The intensities of the features in a neutron spectrum then depend on the amplitude of the vibrations of each atom involved in a particular mode weighted by their scattering power s_l.

EPR spectra were recorded at room temperature using a Bruker ELEXSYS 500 spectrometer (X band). The spectrometer was equipped with a superhigh-Q resonator ER-4123-SHQ and the samples were placed in quartz tubes. In order to stablish a qualitative comparison of the samples was use approximately the same amount of sample and packing degree within the quartz tubes for

all the samples. The magnetic field was calibrated by an NMR probe and the frequency inside the cavity (~9.395 GHz) was determined with an integrated MW-frequency.IR spectra were recorded on a Fourier-transform infrared spectroscopy (FTIR) spectra measurements were carried out using a Jasco FT/IR-6100 spectrometer in Attenuated Total Reflectance mode (FTIR-ATR). Each spectrum was recorded from 400 to 4000 cm^{-1} wavelengths with a 1 cm^{-1} resolution. 64 scans were measured and averaged to obtain the final spectra.

RESULTS AND DISSCUSION

MOF-808 functionalization: Typically, microcrystalline MOF-808 was synthesized as reported in previous works,[48] and the formate ligands exchange performed directly with an aqueous solution of the (amino)acid molecule at a moderate temperature and concentration of the SALE solution (60 ºC, 0.05 M). L-cysteine was selected as a model amino acid to establish the SALE conditions due to its high solubility in water. The volume of the amino-acid aqueous solution and the concentration of the MOF-808 dispersion into the SALE media were fixed to the values reported in the experimental section. In parallel, the concentration of the amino acid solution (*i.e.* 0.05, 0.10 and 0.15 M) was varied to identify the best SALE conditions in terms of the number of cysteine molecules installed per formula unit and the crystallinity of the MOF-808@Cys. To this end, the materials after each SALE cycle were characterized by X-ray diffraction and H^1-NMR. First, we noticed a concentration and temperature dependence for the SALE in MOF-808 up to a maximum of four cysteine molecules incorporated per formula unit. When the cysteine-SALE protocol (80 ºC and 0.15 M cysteine solution) was applied for citric acid, it induced a structural collapse of the MOF-808 framework (Figure S10). Therefore, gentler SALE conditions (60 ºC and 0.5 M citric

acid solution) are necessary to establish a common protocol for all the amino acid functionalities selected to perform this study.

This finding suggests that above a certain temperature and concentration of the (amino)acid solution the citric acid molecules are able to displace the trimesate pillars of the structure, leading to its collapse. As revealed recently by W. Zhang and co-workers,[59] the MOF-808 SALE functionalization is a pK_a-directed process, where acid groups with pK_a lower than the pK_a of the carboxyl groups of trimesic acid, induce the collapse of the framework. Nevertheless, other factors apart from the pK_a, such as the number of acid groups in the molecules incorporated to the framework, may play as well an important role during its collapse, as is the case of citric acid protocol studied in this work. Although the acidity of the carboxyl groups of citric acid (pK_{a1} = 3.13, pK_{a2} = 4.76, pK_{a3} = 6.39, 6.40) are lower than this of the cysteine (pK_a= 1.91), the same SALE conditions induce significant degradation of MOF-808 by citric acid functionalities, while not by the cysteine. We found a similar conclusion when more acidic sulfonic or phosphonic acids were used to encode the MOF-808 at 60 ºC. If the temperature of the SALE conditions is softened to 21 ºC, it was possible to anchor to the MOF-808 very acidic nitrilotris(methylene)tryphosphonic acid (pK_a = 1.09) molecules, with a pK_a value of the phosphonic groups much lower than the threshold marked by the pK_a of the trimesate linkers[59] (Figures S11, S12 and S22).

Taking all these considerations into account, the SALE conditions for the pre-selected (amino)acid functionalizations of MOF-808 were set to: 100 mg MOF per 50 mL water solutionwith an (amino)acid solution concentration: 0.05 M at 60 ºC for 24 h. Afterwards, the successful formate substitution was confirmed by ^{1}H nuclear magnetic resonance (^{1}H-NMR) of the digested samples (Figure 2c and Figures S13-21). The samples were characterized as well by means of X-ray diffraction, IR-spectroscopy, N_2 adsorption isotherms at 77 K and thermogravimetric

measurements. The final formula for MOF-808@(amino)acids were obtained taking into account the BTC:(amino)acid molar ratio obtained by H^1-NMR, and the trimesic linker defect of the parent MOF-808 determined from the weight loss processes observed in the TGA measurements, as detailed in the following.

X-ray diffraction data confirmed the chemical stability of the framework after its (amino)acid decoration (Figure 2b and Figures S1-9). Meaningful displacement of intensity variations of the diffraction maxima have not been observed. These lack of disturbance of the X-ray diffraction signal evidences that the crystal structure of MOF-808 remains mostly unaltered after SALE, and hence, that the (amino)acid molecules exhibit a large degree of disorder within the mesopores. These experimental results are in line with the single crystal X-ray diffraction study performed by Baek *et. al.*[19] for the histidine modified homologue compound; where a highly dispersed electron density map could be attributed to the amino acid molecules at the pore space of the highly symmetric zirconium trimesate framework.

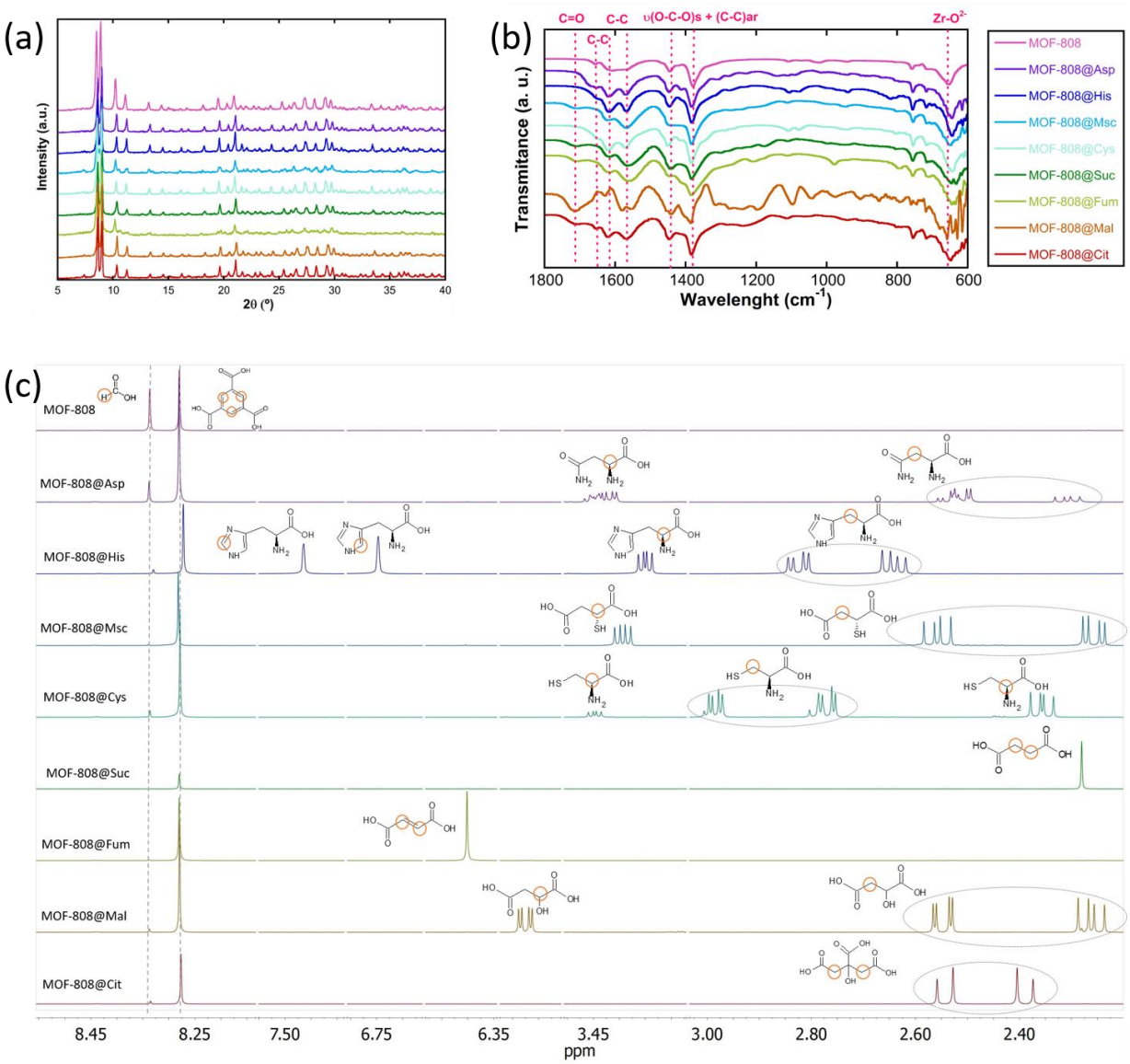

Figure 2. (a) IR spectra, (b) XRD patterns, and (c) ^{1}H-NMR spectra of the digested MOF-808 samples with L-asparagine, L-histidine, mercaptosuccinic acid, L-cysteine, succinic acid, fumaric acid, malic acid and citric acid functionalities.

The IR spectra of the samples (Figure 2a and Figures S33-48) show the additional bands associated to the vibrational modes of the (amino)acid functionalities (i.e. -SH, NH_2, -COOH). Particularly

noteworthy is the absence of the υ_{est}(C=O) vibrational mode (~1700 cm^{-1}) for mono-carboxylate amino acids (*i.e.* His, Asp and Cys). The deprotonation of the carboxyl groups during SALE indicate that this bridging group links the amino acids to the zirconium oxo-clusters of the MOF-808 framework, as corroborated in previous studies by single crystal X-ray diffraction.[44] In contrast, di-carboxylate (*i.e.* Suc, Fum, Mal and Msc) and tri-carboxylate (*i.e.* Cit) acids are predicted to bind to the zirconium clusters only via one of their carboxylate groups, while non-connected carboxyl residues will remain protonated, as confirmed by the IR absorption band associated to the υ_{est}(C=O) vibrational mode (Figure 2a and section S1.4).[60–62] Thermogravimetric curve for MOF-808 (Figures S24-32) shows three weight loss stages associated to: (*i*) the water release (30 – 100 °C), (*ii*) the loss of formate groups and dehydration and dihydroxylation of the zirconium clusters, (125 – 300 °C) and (*iii*) the calcination of the trimesate bridges (425 – 550 °C). As reported by Shearer *et al.,*[63] the zirconium hexanuclear clusters of the UiO-66 structure are completely dehydrated and dehydroxylated at 400 ºC. Thus, the linker deficiency of this zirconium MOF can be calculated by considering the chemical equation of the aerobic decomposition of the dehydroxylated UiO-66 (*i.e.* $Zr_6O_6(BDC)_6$). A similar approach can be applied to estimate the linker defects in MOF-808 if we assume that the zirconium clusters of the materials are fully dehydrated and dehydroxylated at 400 ºC (Figure S24).[64–66] To this end, the theoretical weight loss associated to the linker calcination can be calculated taking into account the following reaction:

$$Zr_6O_{9+1.5x}(BTC)_{2-x} \rightarrow Zr_6O_{12} + (CO_2)_{18-2x} + (H_2O)_{6-3x};$$

where x is the linker defects of the MOF-808 framework; and compared to the experimental ones obtained from the thermogravimetric analysis (Figure S24). By following this approach, 0.08(5) defects per formula unit has been determined. For MOF-808(amino)acid samples, the degree of overlapping between the thermal release of (amino)acid molecules and the trimesic acid

calcination is too high to clearly stablish the temperature where the dehydroxylated $Zr_6O_{9+1.5x}(BTC)_{2-x}$ is formed (Figure S25-S32), and hence, to accurately calculate if the trimesate linker deficiency is enhanced as a consequence of the SALE process.

The composition of the amino acid-loaded MOFs was determined through liquid-state ^{1}H-NMR of the MOFs hydrolyzed via a deuterated NaOH solution. To determine the loading of amino acids, the integrations of amino acid signals were compared to the signals of the BTC linker. As the trimesate linker defectiveness in the MOF-808(amino)acids samples could not be accurately determined, we assumed the same linker defects per formula unit after SALE. As concluded by the ^{1}H-NMR analysis, 3 to 5 of the six available sites per cluster where replaced by (amino)acid functionalities (Table 1). As revealed by N_2 adsorption isotherms at 77 K, the porosity was preserved after SALE. A reduction of the BET surface area and pore diameter is associated as a consequence of the MOF chemical encoding (Figures 2 and section S1.5 in the SI), but mesopore space is still highly available after the amino acid decoration of the framework.

The MOF-808@amino-acid system has been explored and expanded very recently by J. Baek *et al.* [19] and H. Lyu *et al.*[67]. The first authors studied the decoration of the MOF-808 pore space with histidine functions, metallating the system to engineer a pseudo-enzymatic like copper oxidase. The authors were able to incorporate three histidine molecules per cluster via an organic solvent SALE protocol. H Lyu *et al.* have extended very recently the MOF-808@amino acid system to glycine, sarcosine, l-alanine, dl-alanine, (R)-3-aminobutanoic acid, (RS)-3-aminobutanoic acid, l-isoleucine, l-serine, l-histidine, l-threonine and dl-lysine by applying a water SALE protocol with optimized temperature and concentration conditions to achieve the higher degree of functionalization of MOF-808 as possible. H. Lyu *et al*. installed from 2 to 4 amino acid molecules per cluster (except for MOF-808@glycine materials) by modulation the concentration of the amino

acid and the temperature of the media during the SALE. These NMR data is very similar to the one obtained in our work, but still different when comparing the four histidine molecules per cluster of this investigation with the 5 molecules per cluster incorporated in our study. These differences tell us how sensitivity could be the SALE functionalization to experimental conditions as the reactor volume or the concentration of the MOF dispersion into the SALE media.

MOF-808@(amino)acid structure: MOF-808 is built from cuboctahedron $Zr_6O_4(OH)_4(-COO)_{12}$ clusters connected to six homologue inorganic units through benzenetricarboxylate (BTC) linkers (Figure 3a-b).[68] The spatial arrangement of the inorganic and organic building blocks into the MOF-808 structure generates a three-dimensional framework with adamantane shaped pores of a 18 Å diameter.[14] The zirconium clusters are located at the vertices of the hexagonal shaped gates that give access to the inner space of the adamantane pores. The six equatorial plane positions of the clusters are coordinated by six formate groups that point to the center of the pore window. The metrics of the MOF-808 pore entrance are ideal to replace by SALE the formate anions and install small to medium size-molecules, as illustrated in the Figure 3c.[14,48,69] This is the case of the eight natural acids (i.e. succinic (Suc), fumaric (Fum), citric (Cit), L-malic (Mal) and mercaptosuccinic (Msc) acids), and amino acids (L-asparagine (Asp), L- histidine (His) and L-cysteine (Cys)) that we have selected to decorate the pore space of the MOF-808 in this research (Figure 3c).

Taking into account the bridging modes observed for carboxylate and amino acid molecules installed into the MOF-808 structure in previous works,[14] we have constructed tentative structural models for MOF-808(amino)acid variants assuming that *i*) the most acid carboxyl group of the (amino)acid is the one that binds the zirconium oxo-clusters, *ii*) the (amino)acid coordinated the zirconium clusters via its carboxyl group, and *iii*) the (amino)acids are spatially arranged (*i.e.* bond distances, angles and torsion angles) to prevent unreasonable contacts between them within the

pore space.[19] Even though the models lack the backup of single crystal X-ray diffraction experimental data, they aid to visualize and analyse the possible disposition of the (amino)acids within the pore space after the SALE, and the possible distances between the functional groups of adjacent molecules that could bind the same metal-ion during adsorption.

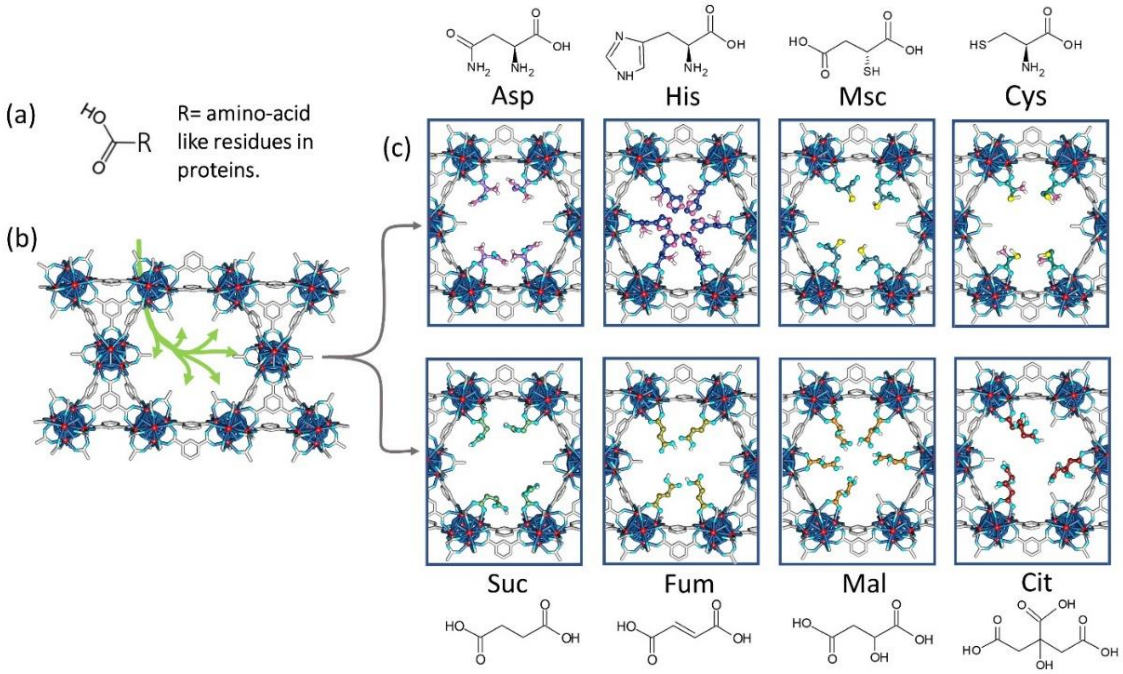

Figure 3. (a) Simplified structure of amino-acid like residues. (b) Installation of amino acid functionalities by solvent assisted exchange into MOF-808 scaffold. (c) Illustration of the pore environment of MOF-808 after its decoration with L-asparagine (Asp), L-histidine (His), mercaptosuccinic acid (Msc), L-cysteine (Cys), succinic acid (Suc), fumaric acid (Fum), L-malic acid (Mal), and citric acid (Cit). Atom labelling scheme of the MOF structure: C, grey; O, red, Zr, blue; N pink; S yellow. H atoms are omitted for clarity. Amino acid functionality has been drawn with different colors to highlight their possible spatial disposition within the MOF-808 scaffold.

It is important to point that, at a first sight, the chemical and conformational flexibility of succinic, fumaric, malic, and mercaptosuccinic molecules may lead to the impression that they could act as bidentate linkers connecting two of the open sites of the same Zr_6 clusters. Nevertheless, the geometric disposition and the distance between the uncoordinated positions at the zirconium clusters makes that even in a highly distorted configuration, these C_4 acids are far to bind the two adjacent linker-defective positions of the same zirconium cluster (Figure S77). Even in the case of a highly distorted C_5 molecule as citric acid, the free carboxyl molecules are far to bind two adjacent positions of the same cluster (Figure S78). It is important to note as well, that the same SALE process could induce to some extent the displacement of some of the trimesate linkers by amino acids or C_4 and C_5 acids used in this study without destabilizing the framework.

At a first sight, the metal capture within the (amino)acid decorated pore space of MOF-808 could occur via (*i*) a single molecule – metal coordination, or (*ii*) cooperatively, when two or more (amino)acid molecules binds the same metal ion. Single (amino)acids can coordinate metals in monodentate -μ_1 or bidentate -μ_2 fashions (Figure S79-80). Instead, a cooperative metal-adsorption will depend on the chemical conformation and disposetion of the amino acids within the MOF-808. For example, for C_3 and C_4-molecules anchored to opposite clusters within the framework, even if they acquire a *trans* conformation, distance between the pedant groups pointing to the pores would range from 7 to 9 Å approximately. This distance is too long to generate (amino)acid-metal-(amino)acid bridges during adsorption. Contrary, the distance of the binding groups pointing to the pore space of the MOF-808 in C_3 and C_4-molecules anchored to adjacent clusters could be short enough (3-5 Å) to trap metals in a bidentate fashion (Figure S81). Contrary, the imidazole groups of histidine molecules installed in opposite positions within MOF-808 pore window exhibits an imidazole – imidazole distances (*i.e.* 4.5 – 5.5 Å) in the range of many metal-imidazole

compounds found in the Cambridge Structural Database. A similar scenario is found for MOF-808@Cit compound, where the distance and conformational flexibility of citrate anions open the perspective to found carboxyl-carboxyl distances within the ranges of the ones found in monomeric, dimeric or trimeric metal-carboxylates.

Chemical stability: The assessment of the chemical stability of MOF-808@(amino)acids is key establishing their window of applicability for water remediation and metal-separation purposes in different scenarios. The chemical stability of the MOF-808@(amino)acids was studied by immersing the samples in water solution with different acidities (pH = 4, 3 and 2) during 24 h. The crystallinity and functionalization degree of the samples before and after their immersion in acidic aqueous media were studied by means of means of XRD and ^{1}H-NMR (Figure 3 and section S2.2). The same experimental procedure has been applied to the MOF-808 for sake of comparison (Figure S58). From the structural stability point of view, all the materials, including the parent MOF-808, are robust enough to keep their diffraction signature after immersing them in acid conditions. The exception to this experimental evidence are MOF-808@His and MOF-808@Asp, which diffraction patterns show a significant broadening of the diffraction maxima. In parallel, the chemical stability of the molecules installed by SALE in the MOF-808 depends on the (amino)acid nature itself. Except MOF-808@His and MOF-808@Msc compounds, the MOF-808@(amino)acids show good chemical stabilities, with minor release of the (amino)acid functionalities (Figure 4 and Figure S59-66). In addition, MOF-808@His is more sensitive to acidic media, showing an appreciable broadening of the X-ray diffraction maxima and nearly complete loss of the (amino)acid molecules when exposed to highly acidic media (pH = 3 and 2) (Figure 4 and Figure S59). In contrast, even if MOF-808@Msc shows an appreciable loss of the

Msc molecules at acidic media, the XRD pattern maintain the crystallinity (Figure 4 and Figure S65).

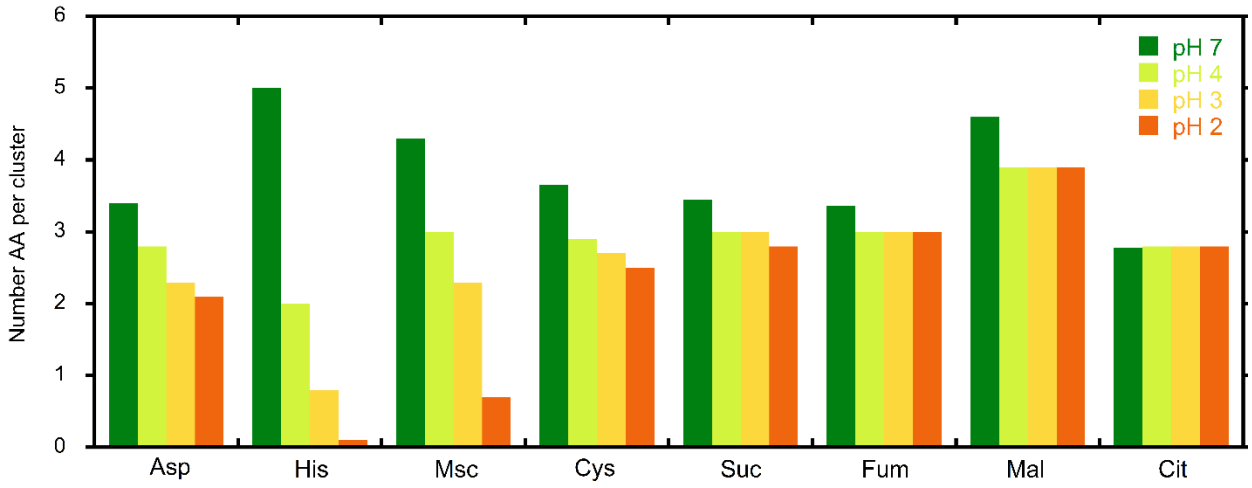

Figure 4. Variation of (amino)acid functionalities per formula unit after immersing MOF-808@Cys, MOF-808@His and MOF-808@Cit in water acidic solutions during 24 h.

It is still unclear why the chemical stability of (amino)acid functions varies if similar anchoring mechanisms of the (amino)acids to the MOF structure are expected. At a first sight, the stability of the MOF-(amino)acid bridges may be defined by the pK_a of the carboxyl groups of the (amino)acid molecules. Nevertheless, no rationale can be found considering only this parameter, since pK_a values for carboxyl groups of His, Cys or Asp are quite similar, and their chemical stabilities when installed in the MOF-808 frameworks differs significantly. A possible explanation for MOF-808@His compound could be a charge-balance related destabilization triggered by a protonation of amine groups (pK_a = 6) when the pH is below 6. Still this cannot explain the chemical instability of Msc functions.

The stability over the presence of highly coordinating sulphate anions was as well tested for MOF-808@Cit compound, since this variant is the one exhibiting the lower loss of crystallinity and

citrate release in acidic media. MOF-808@Cit was immersed in 1 M Na_2SO_4 solution (96 ppms of sulphate concentration) of pH = 3 during 24 h. As concluded from the XRD data, the compound is partially transformed to another phase during the process (Figure S67). Nevertheless, the trimesic to citric acid molar ratio obtained by ^{1}H-NMR after the transformation is very similar to the citrate molecules per zirconium cluster observed for the parent compound. So, the presence of an elevated concentrations of highly coordinating anionic species as sulphate induces the degradation of a significant weight fraction of the MOF-808@Cit framework, but the citrate groups in the MOF-808@Cit that is still crystalline after the process are stable enough to remain anchored to the framework.

The chemical stability of MOF-808(amino)acid materials allows advancing the horizon of applicability of these materials for the recovery of metals from aqueous environments. First, the robustness of the SALE encoding opens the perspective to the application of MOF-808(amino)acids for surface water decontamination purposes, but not for the recovery of metals from seawater (e.g. uranium adsorption), or from acid-waters derived from phospho-gypsum deposits, since the sulphate content in this media is above the stability threshold of our system. Second, the acid-stability of MOF-808@(amino)acids may enable the recovery of metals from acid leachates derived from metal-recycling or mining activities, but not if the anionic strength of highly coordinating oxyanions (*e.g.* sulphate, phosphate, chloride…) in the solutions is above the chemical stability limit of the MOF-808(amino)acids.

Metal adsorption affinity: Single-ion adsorption tests were performed with MOF-808@(amino)acids in acidic solutions (pH ≈ 4) of 100 ppm metal concentration. To this end, 100 mg of MOF-808@(amino)acid was immersed in 50 mL of Hg(II), Pb(II), Cd(II), Cu(II), Ni(II),

Eu(III), Cr(III), and Cr(VI) 100 ppm solutions while monitoring the metal concentration before and after the sorption equilibrium. Metal ions were selected on the basis of their acidity (Z/r^2- Soft-Intermediate and Hard), coordination environment, and charge. Adsorption capacity was calculated as mmol of metal adsorbed per mol of sorbent (Figure 5). Except Cr(VI), all the metal ions are found in their cationic forms in water solutions. In the specific case of Cr(VI), it is stabilized as $(Cr_2O_7)^{2-}$ and $(HCrO_4)^-$ anions at the acidic conditions studied in this work.

Unmodified MOF-808 welcomes Cr(VI) adsorption since its chromate anionic form is able to displace formate anions to bind the zirconium hexa-nuclear clusters (Figure 5a).[70] The mechanism of MOF-808 capture of Cu(II) and Cr(III) intermediate and hard ions is still unclear. Nevertheless, previous researches have installed copper and chromium oxo-aqueous species covalently bonded to the zirconium clusters through solvent vapor deposition.[71]

Once the (amino)acid functionalities are installed within the MOF-808 framework, its ability to capture metal ions changes drastically (Figure 5b-i). As a general rule, the adsorption affinity of the MOF-808@(amino)acid samples over cations can be explained by Pearson acid-base theory,[72] that is, soft acidic metal ions tend to interact with soft basic functional groups, and vice versa. However, this is not the unique parameter governing the adsorbing affinity of MOF-808@(amino)acid system, as the number of amino acid residues and their spatial disposition shape as well the affinity of the system to trap metal ions far from the general trends described by the Pearson Rule.

When histidine is installed at the MOF-808 framework, amino and imidazole functionalities decorate its inner pore structure enabling the capture of soft intermediate metal ions as Hg(II), Pb(II) and Cd(II) (Figure 5c).

Similarly, the combination of thiol-amine, and, thiol-carboxyl residues in MOF-808@Cys and MOF-808@Msc give rise to the concurrent adsorption of weak (Hg(II), Cd(II) and Pb(II)) and intermediate (Cu(II), Ni(II)) metal ions (Figure 5d-e). In comparison to His and Asp based MOF-808, Cys and Msc homologues capture Ni(II) ions too, which is an ion slightly more acidic than Cu(II). The installation of carboxyl and hydroxyl residues within the MOF-808 through its functionalization with succinic, fumaric, malic and citric acids give access to trap intermediate to hard metal ions, as Cu(II), Ni(II) and Eu(III) (Figure 5f-i). Indeed, complex functionalities combining several carboxyl and hydroxyl groups (i.e. malic and citric acid) work more efficiently than functionalities based on single carboxyl residues (Figure 5h-i). On the top of that, it is important to mention that it is still a room of improvement to enhance the adsorption capacities towards these hard ions by including sulphonyl or phosphonate groups within the framework, as reported in previous works.

The capture of Cr(VI) and Cr(III) by MOF-808@(amino)acids seems to be governed by factors beyond the general hard-soft acid-base rule. As previously mentioned, Cr(VI) is a chromate anionic form in solution, so anion exchange by formate anions is predicted to be the preferred adsorption mechanism in non-functionalized MOF-808 (Figure 5a). For instance, carboxylate type functionalizations (*i.e.* Suc, Fum, Mal, and Cit) significantly reduce the adsorption capacity of MOF-808 to capture Cr(VI) since chromate is not able to displace them and access the preferred chemisorption positions at the zirconium clusters (Figure 5f-i). This is especially notorious in MOF-808@Cit, as electrostatic repulsions and stearic impediments can further impede Cr(VI) uptake. Counterintuitively, amino acid decorated MOF-808 materials exhibit similar adsorption capacities over Cr(VI) than parent MOF-808. Chromate uptake by these functional groups can be explained on the basis of two different mechanisms, (*i*) the electrostatic adsorption by $-NH_3^+$

protonated groups in His, Cys and Asp functionalities,[54] and (*ii*) the chemical reduction of Cr(VI) to Cr(III) by the electron donation of thiol and amine groups.[73] This dual adsorption/chemical reduction mechanism over chromate anions has proven to be highly effective for amino and hydroxyl UiO-66 variants.[2]

The adsorption affinity of MOF-808@His and MOF-808@Asp over Cr(III) is counterintuitive, since highly acidic ions (such as trivalent chromium) prefer to coordinate carboxyl hard functionalities (*i.e.* MOF-808@Cit and MOF-808@Mal). However, MOF-808@His and MOF-808@Asp exceeds by much the capacity to capture Cr(III) (1600 mmol/mol and 500 mmol/mol) in comparison to the MOF-808 counterparts functionalized with carboxyl acid residues.

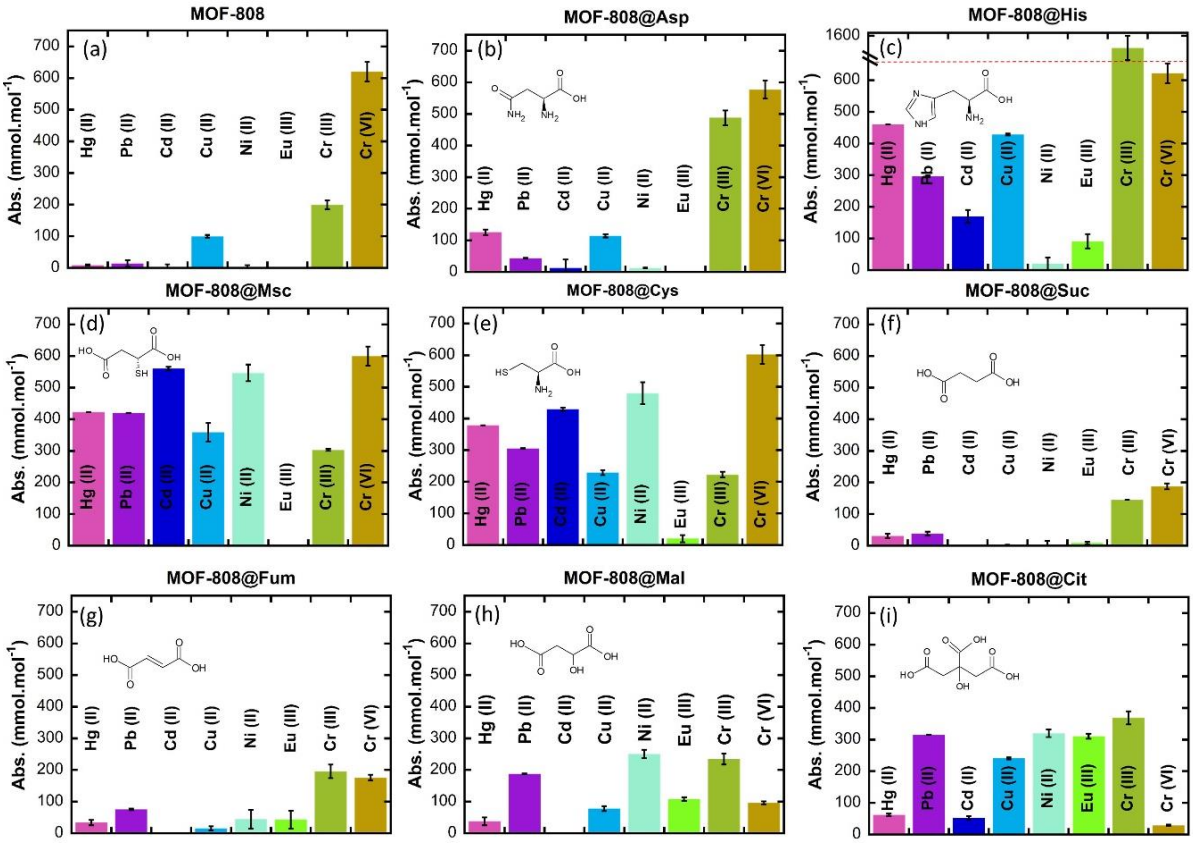

Figure 5. Adsorption capacity ($mmol \cdot mol^{-1}$) of the different MOF-808@(amino)acid samples over Hg(II), Pb(II), Cd(II), Cu(II), Ni(II), Eu(III), Cr(III), and Cr(VI). Experiments were performed with an initial metal ion concentration of 100 ppm, using 2 mg MOF/mL.

The capacity to adsorb the same metal-ions from a multielement solution was determined for all the studied materials. The results have been plotted in terms of distribution coefficient factors (K_ds) (calculated as detailed in the experimental section). K_d values of each adsorbent for each metal allows easily visualizing the efficiency of the sorbent to extract the metal from the solution. In addition, the separation factor of a sorbent can be obtained by calculating the ratio of the K_ds values for different metals (see experimental section for more information). The linear plot of the K_d values shown in the Figure 6a clearly reveals the more affine sorbent – metal pairs (*i.e*. MOF-808@Cys-Hg, MOF-808@Cys-Cu, MOF-808@His-Cr and MOF-808@Cys-Hg), all of them with K_d values above 10^5. If the data is plotted in a logarithmic scale (Figure 6b), these sorbent-metal pairs with K_d values below 10^{-5} are revealed. Although less efficient than the sorbent-metal pairs identified in the Figure 6a, K_d values from 10^{-3} to 10^{-5} are still interesting, especially for the later computing of separation factors. Following the same tendency than for single-element adsorption tests, two families of MOF-808(amino)acid materials can be distinguished, the Msc, Cys, His and Asp variants able to capture soft to intermediate metal ions, and the Cit and Mal functionalized compounds, which metal-affinity is shifted towards hard metals as the trivalent REE. Therefore, taking into account the K_d values, the first group of MOF-808@(amino)acid materials are appealing from water remediation of the three of the heavy metals (Pb(II), Cd(II), Hg(II)) included in the big-four defined by the World Health Organization. Giving the differences in the K_d values for soft and hard metal ions, the separation of heavy metals Msc, Cys, His and Asp MOF-808

variants. Last but not least, although the K_d values of MOF-808@Cit or MOF-808@Mal for REE are low, some of the calculated separation factors between Eu(III), Y(III) and La(III) start to be interesting for individual REE separation. Nevertheless, further development of the MOF-808 pore chemistry is needed to improve them.

Breakthrough experiments: Breakthrough experiments with the multielement solution flowing over a sand-packed bed of MOF-808@(amino)acid were performed with a flow rate of 0.5 $mL \cdot min^{-1}$. As expected, the metal-affinity of each MOF-808@(amino)acid alters the breakthrough volume of each metal in the column (Figure 6d-l). The experimental data have been fitted to the Thomas model, and the adsorption capacity and the Thomas constant values for each Sorbent-Metal pair summarized in the Table S5.

Continuous flux adsorption experiments show that the parent MOF-808, Suc and Fum variants show negligible retentions times for soft to hard metal-ions, so all the studied elements cross the column without a delay time. For Cys, His, Msc and Asp materials, the breakthrough time of the soft and intermediate metals in the output of the column is delayed significantly in comparison to hard ions. Within the intermediate and soft ions studied, the order and the volume of the column rupture for each metal varies significantly depending on the MOF-808 functionalization. For example, MOF-808@Msc and Cys columns are able to detoxify from 300 to 500 mL of a 10 ppm Hg(II) solution lowering the mercury concentration below the legal limits stablished by WHO, but the breakthrough volumes for Cd(II) or Pb(II) are lower than the ones of Hg(II). Event though, the terminal concentrations of Cd(II) and Pb(II) before the rupture of the column are lower as well than the legal threshold defined by WHO as well.[74]

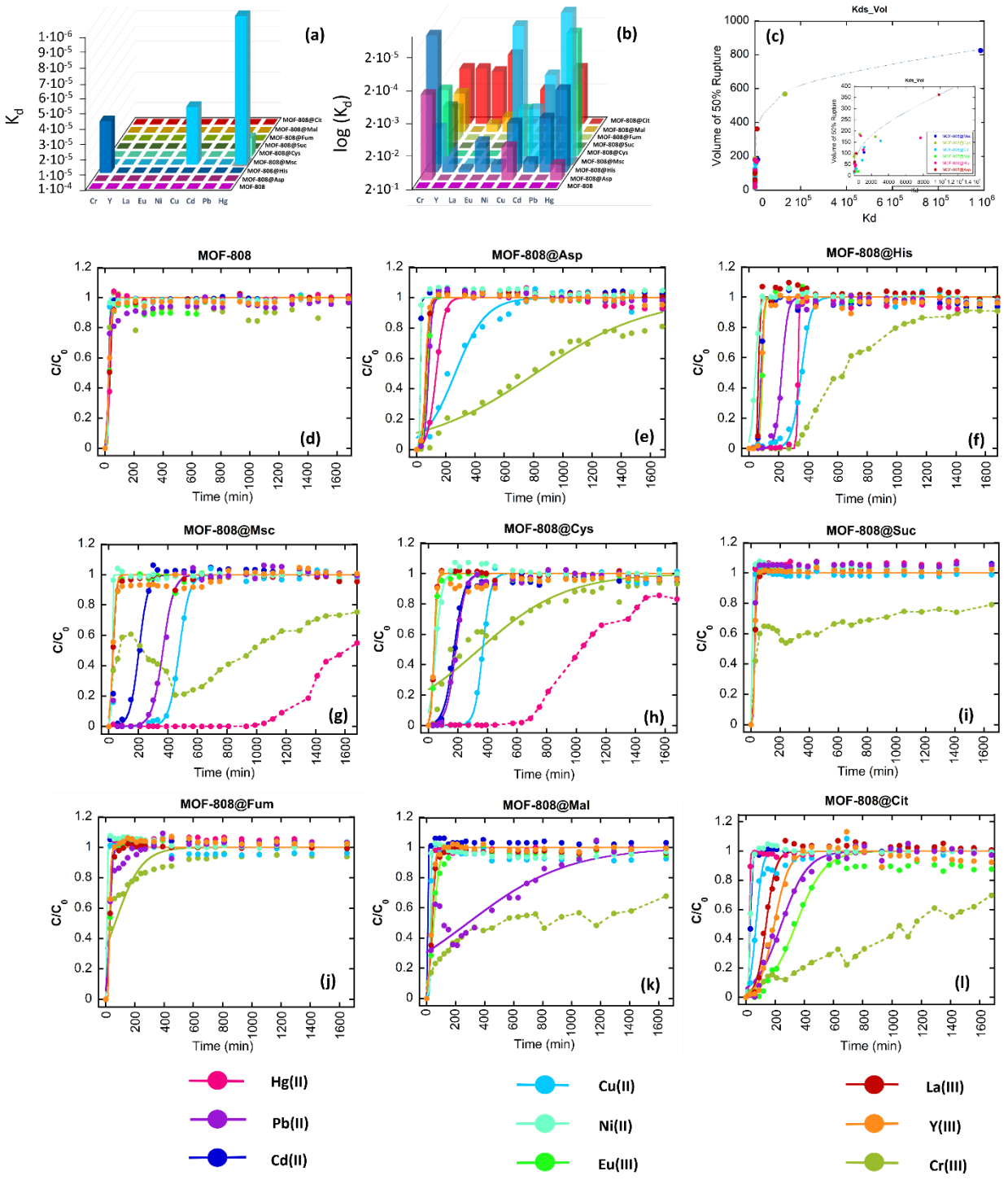

Figure 6. (a-b) Metal distribution coefficients for MOF-808(amino)acid samples obtained from the adsorption experiments in a multielement solution of Cr(III), Y(III), La(III), Eu(III), Ni(II), Cu(II), Cd(II), Pb(II), and Hg(II) ions. The data have been plotted in (a) linear and (b) logarithmic

scale basis. Experiments were performed with an initial metal ion concentration of 10 ppm, using 2 mg MOF/mL. (c) Correlation between the Kd values and the volumes at C/C_0 in breakthrough experiments. (d-l) Breakthrough curves of of the different MOF-808@(amino)acid samples over a multielement mixture. Experiments were performed with an initial metal ion concentration of 10 ppm, using a packed bed column of 100 mg of MOF in 1.5 g of sand, and with a flux of 0.5 $mL \cdot min^{-1}$.

In parallel, the incorporation of carboxyl and hydroxyl groups in MOF-808@Mal and MOF-808@Cit variants have an opposite effect of the breakthrough experiments. In these cases, the times of column ruptures for acidic metal ions are increased, whilst the soft metal-ions pass the column without delay time. For instance, a quite interesting separation capacity for different rare earth elements is starting to be observed for MOF-808@Cit variant. It is important to note the uncommon behavior of Cr(III) on the static adsorption and breakthrough experiments in multielement solutions that may be related to its precipitation due to its long-term stability in solution. Interestingly, the value of the volume at $C/C_0 = 0.5$ for each metal has been related with the K_d value of each MOF-808@(amino)acid – metal pair (As shown in the Figure 6c). The logarithmic tendency suggests that a slight increase in the K_d value for a given metal led to an exponential delay of its breakthrough time in the column.

The feasibility of MOF-808@(amino)acids as water remediation technology against heavy metals pollution (i.e. Cd(II), Hg(II) and Pb(II)) was evaluated as well through kinetics and isotherm adsorption experiments for MOF-808@Cys and MOF-808@His. Adsorption kinetics studies reveal extremely fast capture with equilibrium times below 2 min (Figure S68). Adsorption

isotherms indicate a maximum adsorption capacities up to of 40 mg/g for Cd(II) (MOF-808@Cys), 175 mg/g for Pb(II) (MOF-808@His) and over 350 mg/g for Hg(II) (MOF-808@Cys and MOF-808@His) (Figure 7a-f). That is, at its maximum loading capacities, the MOF-808@Cys variant is able to host 1.35 Pb(II), 1.9 Hg(II) and 0.55 Cd(II) ions per formula unit.

Langmuir and Freundlich models were applied to fit the experimental data (Section S3.1) and in order to better quantify the adsorption capacity and affinity of His and Cys modified MOF-808 over Cd(II), Hg(II) and Pb(II). The slightly better fitting of the experimental curves to the Freundlich model suggest a homogeneous binding of the metal ions to the MOF-808@(amino)acids functionalities. Nevertheless, Pb(II) and Cd(II) capture can be related to their coordination by imidazole and amino functionalities, as it can be observed in many Pb(II) and Cd(II) amino acid metal complexes. In comparison, given the tendency of Hg(II) to form Hg(II)-S bonds, their coordination to thiol and imidazole residues of Cys and His is the most plausible mechanisms for the capture of soft ions.

The performance of MOF-808@aminoacid, both in terms of adsorption kinetics and capacity, is close to the best values reported for MOFs materials so far (Figure 7g), and rivals the values reported for sorbents as functionalized-carbon, polymers or zeolites.[56,75] MOF-808@Cys was also tested under static adsorption conditions to capture Hg(II), Cd(II) and Pb(II) from solutions with concentrations (*i.e.* 1 ppm) closer to those usually observed in polluted water sources (Figure S69). An adsorption efficiency above 99.99 % was obtained for Hg (II), reducing its concentration from 1 ppm to 0.002 ppm, a value bellow the legal limit (0.01 ppm) established by the World Health Organization (WHO).[74] The performance of MOF-808@Cys to capture Pb(II) and Cd(II) ions is also outstanding, with uptakes above 98% of the initial metal ions content, reaching concentrations close to 0.1 ppm after adsorption. Adsorption conditions can be easily improved by increasing the

MOF loading (current = 2 mg MOF/mL) to achieve the concentration thresholds stablished by WHO for Pb(II) (0.001 ppm) and Cd(II) (0.003 ppm).

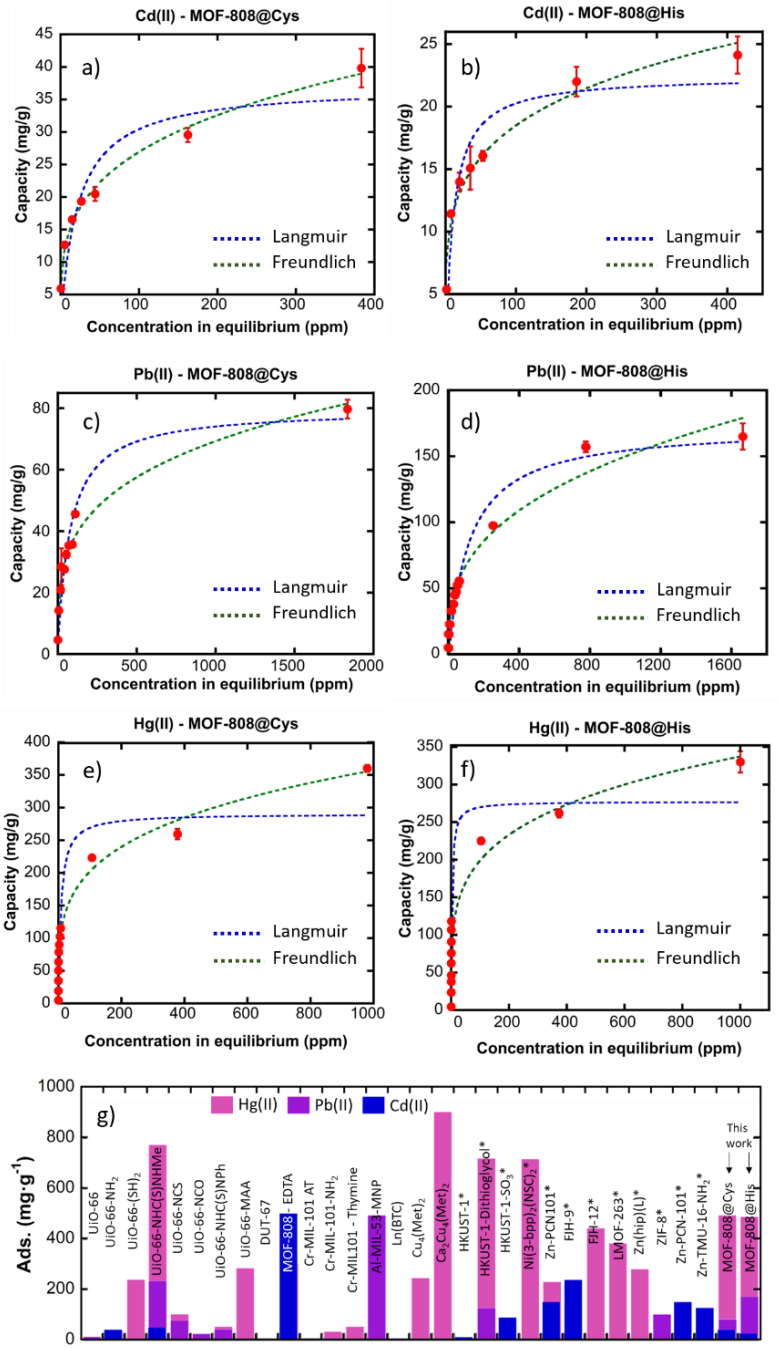

Figure 7. Adsorption isotherms for MOF-808@Cys and MOF-808@His over (a-b) Cd(II), (c-d) Pd(II), and (e-f) Hg(II). Dashed lines, blue- Langmuir fitting, green - Freundlich fitting. (g)

Comparison of the MOF-808@His and MOF-808@Cis maximum adsorption capacities over Hg(II), Cd(II), and Pb(II) with previously studied MOFs.

Metal speciation - the case study of MOF-808@Cys and MOF-808@His

Copper was selected as ion-probe to monitor its color and the electron paramagnetic spectroscopy fingerprints once immobilized by MOF-808@(amino)acids. Copper compounds exhibit characteristic colors that are easily linked to its coordination environment and oxidation state. First, during adsorption, the color of the MOF-808@His and MOF-808@Cys dispersions, once immersed in the $CuCl_2$ (100 ppm) solution, were monitored. A fast and drastic color change from green pale ($CuCl_2$) to pale blue and pale-brown was noted in MOF-808@His and MOF-808@Cys dispersions respectively, and 3 hours after the adsorption, MOF-808@His-Cu acquired a more intense blue color (Figure S70-71). The blue color of MOF-808@His-Cu is in good agreement with copper histidine coordination compounds.[76,77] Contrary, the pale brown suspension obtained after the addition of MOF-808@Cys suggests that the copper coordination via thiol groups is coupled to its partial reduction. For sake of comparison, similar experiments were conducted with Cr(III), and Cr(VI) metal ions with Cys functionalized materials. This time, the color of the MOF-808@Cys-Cr(VI) sample in agreement with the yellow color of the potassium dichromate solution. However, the system evolved after some minutes to the characteristic pale-green color of Cr(III), which led us to think that Cr(VI)→ Cr(III) reduction happened concurrently with the Cr(VI) adsorption (Figure S72).[2] Just from the visual inspection of the color evolution, and considered the characteristic UV-Vis adsorption fingerprints of the studied metals (*i.e.* coordination environments, oxidation…), it can be concluded that metal immobilization in MOF-

808@(amino)acid system does not only involve amino acid — metal coordination chemistry, but electron transfers processes able to reduce and oxidize the immobilized metal ions.

EPR spectroscopy help us to gain further insights about the metal coordination on MOF-808@aminoacid system. MOF-808@Cys-Cu and MOF-808@His-Cu exhibit the characteristic EPR fingerprint of magnetically isolated Cu(II) complexes with a tetragonal ligand field environments (Figure 8a-b and figure S73).[78] A second signal associated to Cu(II) clustered ions is also observed jointly with the one of isolates species. The fitting of EPR spectra points to $g_{\perp}$ values of 2.274/2.259 2.063/2.062 (His/Cys) and $g_{\parallel}$ values of 2.274/2.259 (His/Cys). The four-line hyperfine structure allows estimating the $A_{\parallel} = 175 \cdot 10^{-4}/183 \cdot 10^{-4}$ cm^{-1} (His/Cys) and $A_{\perp} = 10 \cdot 10^{-4}/15 \cdot 10^{-4}$ cm^{-1} values too. The obtained g and A values are in good agreement with a highly symmetric equatorial square planar coordination geometry formed by two oxygen and two nitrogen atoms. While this conclusion is highly robust for the MOF-808@His-Cu sample, it is surprising when cysteine residues are considered as the chelating molecules of the copper ions in the MOF-808@Cys system. The Cu(II) ions coordination by the thiol groups may involve its partial reduction to Cu(I), making Cu-S based metal centers in MOF-808@Cys silent to be detected by EPR.[79] Therefore, Cu(II) is likely to be coordinated by amine functions. Considering the fact that cysteine amino acid only possesses one amine-group per molecule, the coordination environment suggested by the EPR data points towards the immobilization of the copper ions via at least two different amino acid molecules. In addition, it is important to notice that both MOF-808@Cys-Cu and His-Cu systems exhibit clustered copper ions with g values (*i.e.* 2.10 (His), 2.12 (Cys)) that are close to the average of $g_{\perp}$ and $g_{\parallel}$ observed for the isolated species, so when clustered, the coordination environment of the square planar Cu(II) individual ions is still maintained in the system.[80]

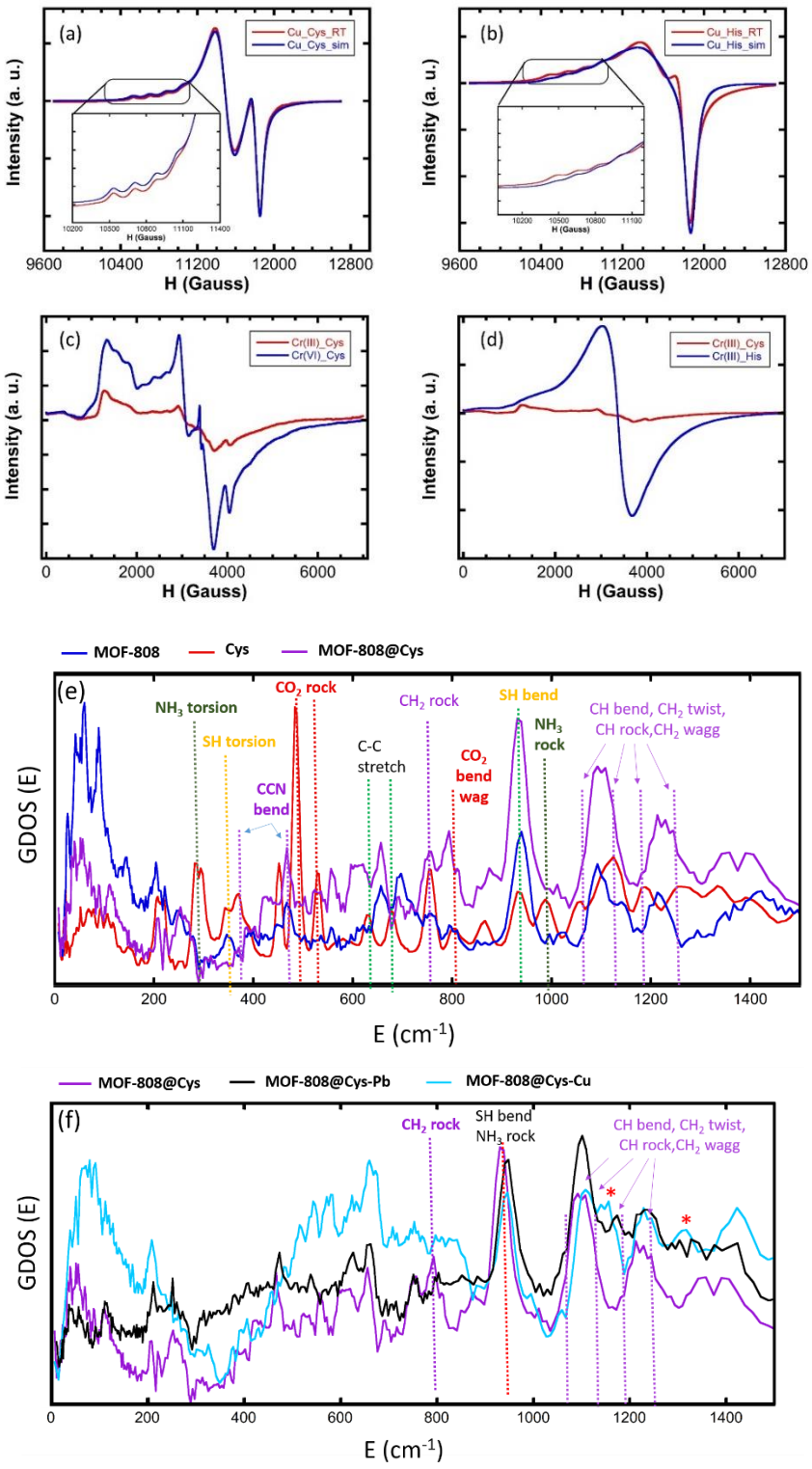

Figure 8. Experimental and simulated Q-band EPR spectra of (a) MOF-808@Cys-Cu, (b) MOF-808@His-Cu at room temperature, (c) MOF-808@Cys-Cr(III)/Cr(VI), and (d) MOF-808@His

and Cys –Cr(III). Inelastic scattering spectra of (e) MOF-808, L-Cysteine and MOF-808@Cys and (f) MOF-808@Cys after Pb(II) and Cu(II) adsorption.

A similar strategy was applied to study the metal speciation of Cr(VI) and Cr(III) ions in MOF-808@aminoacid system by means of EPR. In order to prove the reduction capacity of MOF-808@Cys, Cr(VI) adsorption experiments were conducted. Cr(VI) is silent by EPR, but if it is reduced to its trivalent state, it becomes active. For instance, the presence of the characteristic EPR fingerprint of isolated Cr(III) in MOF-808@Cys sample after the adsorption of Cr (VI) confirms that reduction process is coupled to the metal ion capture (Figure 8c).[70] In fact, the Cr(III) EPR signal is more intense in MOF-808@Cys after adsorbing/reducing Cr(VI) in comparison to the one after the direct Cr(III) adsorption. This is in agreement with the MOF-808@Cys adsorption capacities for Cr(III) and Cr(VI) species shown in the Figure 5e. This trend is further accentuated for the MOF-808@His. The broad and high intense adsorption band for Cr(III) in MOF-808@His (g=1.99) (Figure 8d) is indicative of the clustered Cr(III) ions, which seems logic due to the enormous adsorption capacity that MOF-808@His shows for Cr(III) (1600 mmol/mol - Figure 5c).

Although EPR is highlight sensitive to metal coordination variation, it does not give any direct experimental evidence of the functional groups that are participating in the metal ion capture. As a first attempt, infrared and Raman spectroscopy were used to observe the variations induced by the cysteine functionalization, and the posterior metal adsorption. Nevertheless, the signals associated to the amino acid molecules where highly weak, and no significant changes were observed after the metal immobilization. Inelastic neutron scattering (INS) data was a must to reveal the spectroscopic signals associated to the hydrogen atoms of amino acid molecules

installed into the MOF-808. At a first step, the vibrational bands of the INS data of MOF-808, cysteine and MOF-808@cys samples were identified on the basis of the bibliographic data (Figure 8e).[81]

Among the differences observed between the free Cys and MOF-808@Cys spectra (Figure 8 e), the disappearance of the INS bands associated to the COOH vibrations (CO_2 rock at ~500 cm^{-1}) is in good agreement with the anchoring of the Cys molecules to the zirconium clusters of the framework via the carboxyl groups. In addition, both the disappearance of the NH_3 torsion vibration (~300 cm^{-1}), together with the displacement to lower energies of the other bands associated to the Cys molecule, clearly indicate that once immobilized, the interactions of the Cys with the framework and the adjacent Cys molecules, are altering the vibrational modes of the molecule, blocking even some of the intramolecular vibrations of the molecule.

In order to further validate this interpretation we performed Density Functional Theory (DFT) calculations of the isolated molecules: free cysteine (Figure S83, and a model of two cysteine molecules coordinating a Pb(II) ion in a bidentate fashion(Figure S83, and then the calculated INS spectra were obtained. Although the intensity of the INS signal for these simplified models is not representative of the one that would be obtained in an ordered crystal environment, the energy values associated to the vibrations are accurate enough to stablish qualitative comparisons. Two are the main spectral variations observed when the cysteine is anchored to the MOF: (i) the vibrational modes of COOH and NH_3 disappear, and (ii) the bands associated to the CH, CH_2, and the bending and rocking modes of SH and NH_3 groups, respectively, gain intensity in comparison to the ones of the free cysteine. It is important to note that the signals associated to the bending and rocking modes of SH (~ 975 cm^{-1}) and NH_3 (~ 990 cm^{-1}) groups in free cysteine molecules seem to be shifted to the same position in the MOF-808@Cys compound (~ 975 cm^{-1}).

Among the INS bands affected by the metal adsorption (Figure 8f), the intensity of the signal located at 950 cm^{-1} energy is slightly reduced in comparison to the initial MOF-808@Cys. The band was initially assigned to the combination of the bending vibration of SH and the rocking vibration of NH_3 groups. This band assignment was done taking into account the work performed by Stewart F. Parker *et al*.,[81]., as well as the INS spectra calculated from the vibrational modes of free Cys molecules. In addition to the subtle intensity loss, Pb(II) and Cu(II) adsorption induces a slight displacement of the signal to higher energy values. The metal coordination by sulfide groups by Cu(II) or Pb(II) ions would induce a deprotonation to S^- anions, and thus, to a reduction of the INS signals associated to the SH vibrational modes (~950 cm^{-1}). In contrast, as revealed by many metal-coordination complexes found in the CSD database, the coordination of NH_3 groups to Cu(II) or Pb(II) usually induces a deprotonation of the ammonium to amine, so the vibrational modes associated to NH_2 functions are still active after the metal complexation, although maybe displaced to a slightly different energy values. Thus, revisiting our first assignment of the band located at 950 cm^{-1}, it seems that the SH's vibrational modes contribution is not so relevant as the one of NH_3 rocking vibrational mode to this signal of the INS spectra. This conclusion is based on an active participation of the -SH groups to the metal-chelation of both Pb(II) and Cu(II) ions, that finally would lead to a significant reduction of the intensity of the signal. For instance, the INS spectral simulation performed for a dual bidentate coordination of a Pb(II) ions by two cysteine molecules, as proposed by F. Jalilehvand *et al,*[79], corroborates our hypothesis. In this case, the bands at 913 cm^{-1} and 960 cm^{-1} are related with vibrational modes of the NH_2 and CH_2 groups, while the initial band of free cysteine at 928 cm^{-1} was associated to a combination of the NH_2 and SH vibrational modes (Figure S83).

In parallel, the suppression or the variation of the -CH_2 rocking vibrational mode after Pb(II) and Cu(II) adsorption, as well as the appearance of two new INS signals (1150 and 1325 cm^{-1}), marked with asterisks in the Figure 8, within energy region of CH bend, CH_2 Twist, CH rock and CH_2 wagg vibrational modes for Cu(II) loaded MOF-808@Cys variant, offer the keys to further understand the Pb(II) and Cu(II) uptake mechanisms. Considering the possible Pb(II)-cysteine complexations in solution proposed by F. Jalilehvand *et al.*,[79] a bidentate coordination of the SH and NH_3 groups to the Pb(II) (Figure 8e) could give rise to the complete blocking of the CH_2 rocking mode, since its vibrational freedom would be severely restricted if the metal ion is linked to both SH and NH_3 terminal groups of the cysteine molecules. This binding mode, where SH groups are involved, explain the slight reduction the INS band at 950 cm^{-1}. It is important to note that even if the $PbCys_2$ complex is the most stable form of Pb(II) stabilization in solution, as revealed in many coordination compounds found in the Cambridge Structural Database Pb(II) ions prefer the coordination via amine in comparison to thiol groups. In contracts, copper complexation by cysteine seems to be governed by its preferential binding to the thiol groups. A Cu-S-Cysteine monodentate binding mode (Figure S79), or even a dual coordination of the copper ions by two adjacent cysteine molecules via S-Cu-S bridges (Figure S82), would suppress the CH_2 rocking vibrational mode, but also give rise to the modification of the CH bend, CH_2 Twist, CH rock and CH_2 wag vibrational modes in comparison to MOF-808@Cys-Pb(II) compound, as observed in the experimental INS spectra. For instance, in addition to the main population of copper ions stabilized as Cu(II) and Cu(I) within the MOF-808@Cys via cysteine groups, it is important to take into account that there is a population of copper ions that are coordinated as well via amine groups, as revealed by EPR spectroscopy.[82] This dual stabilization mode of copper could explain

the complexity of the INS region CH bend, CH_2 Twist, CH rock and CH_2 wag vibrational modes in comparison to the initial MOF-808@Cys and MOF-808@Cys-Pb(II) compounds.

In general terms, copper immobilization by MOF-808@aminoacid goes further than a simple metal coordination process found in metal-chelator systems, since it involves electron transfer and metal redox mechanisms. This point was further confirmed by voltamperometric measurements of MOF-808@His, Cys and multivariate MOF-808@His-Cys samples after the immobilization of copper ions (Figure S89-S91). The electrochemical measurements show a characteristic anodic peak of the Cu(0) to Cu(II) oxidation with potentials of E_0= -97 mV, E_0= -57 mV and E_0=+22 mV for the His, Cys and His/Cys frameworks. On the basis of E_0 values for the copper oxidation, it can be concluded that the redox characteristics of the metal cores within the MOF-808@(amino)acid frameworks can be partially tuned. For instance, the His and Cys multivariate MOF-808 copper oxidation potential is far to be the average of the values found in Cys and His compounds; which suggest that both amino acids are involved in the coordination of the metal ion within the MOF structure. Further research is needed to fully understand the electrochemistry of MOF-metal chelator systems, but these initial findings point out to the versatility and complexity of MOF-amino acid materials to immobilize metal ions exhibiting exotic optic, electronic and redox properties.

CONCLUSIONS

We have demonstrated that the installation of natural and amino acids within a MOF can alter significantly the adsorption capacity and affinity towards metal ions with varied characteristics. In addition, MOF-808@(amino)acids show fast kinetics, and outstanding capacity to capture heavy

metals even in continuous flow conditions. For instance, the adsorption capacities obtained for MOF-808(amino)acids rival the figures of the best MOFs reported up to date for Hg(II), Cd(II) and Pb(II) adsorption. The immobilization of amino acid functions into the pore space of MOF-808 endow the material of metal-complexing mechanisms where single or cooperative metal-binding modes give rise to the stabilization of isolated, clustered, and even, partially reduced species for some specific metals as copper. We anticipate that amino acid encoding, and especially multivariate decoration of MOFs with multiple amino acid residues, will become an important tool in engineering artificial metal-chelator functions with improved selectivity to trap metal ions from complex mixture.

SUPPORTING INFORMATION

The following files are available free of charge.

Detailed description of the samples' characterization techniques and protocols Powder X-ray diffraction (Pag. S3), 1H-NMR (Pag. S9), Thermogravimetric analysis (Pag. S14), IR spectra (Pag. S20), N_2 Adsorption isotherms and BET calculation (Pag. S28), pK_a values of the (amino)acids (Pag. S32). Samples stability assessment by X-ray diffraction patterns of the samples after their soaking into water solutions of different pHs (Pag. S32). Specific protocols and characterization techniques for the development of metal adsorption tests and the post-operation characterization of the materials (Pag. S38).

AUTHOR INFORMATION

Corresponding Author

Stefan Wuttke – BCMaterials (Basque Center for Materials, Applications & Nanostructures), Bldg. Martina Casiano, 3rd. Floor, Barrio Sarriena s/n, 48940, Leioa, Spain. Orcid: https://orcid.org/0000-0002-6344-5782, e-mail: stefan.wuttke@bcmaterials.net

Roberto Fernández de Luis – BCMaterials (Basque Center for Materials, Applications & Nanostructures), Bldg. Martina Casiano, 3rd. Floor, Barrio Sarriena s/n, 48940, Leioa, Spain. Orcid: https://orcid.org/0000-0002-8924-230X, e-mail: roberto.fernandez@bcmaterials.net

Authors

Ainara Valverde – BCMaterials (Basque Center for Materials, Applications & Nanostructures), Bldg. Martina Casiano, 3rd. Floor, Barrio Sarriena s/n, 48940, Leioa, Spain. Macromolecular Chemistry Group (LABQUIMAC), Department of Physical Chemistry, Faculty of Science and Technology, University of the Basque Country (UPV/EHU), Barrio Sarriena s/n 48940 Leioa (Spain) Orcid: https://orcid.org/0000-0002-2219-7516, e-mail: ainara.valverde@bcmaterials.net

Gabriel I. Tovar Jiménez – Facultad de Farmacia y Bioquímica. Departamento de Ciencias Químicas. Universidad de Buenos Aires. Buenos Aires, Argentina. Instituto de Química y Metabolismo del Fármaco (IQUIMEFA). CONICET - Universidad de Buenos Aires. Buenos Aires, Argentina. Orcid: https://orcid.org/0000-0003-1642-4126, e-mail: gabrieltovarj@gmail.com.

Natalia A. Rio-López– BCMaterials (Basque Center for Materials, Applications & Nanostructures), Bldg. Martina Casiano, 3rd. Floor, Barrio Sarriena s/n, 48940, Leioa, Spain. Barrio Sarriena s/n 48940 Leioa (Spain) Orcid: https://orcid.org/0000-0003-4119-6065, e-mail: natalia.rio@bcmaterials.net

Dimas I. Torres – Facultad de Farmacia y Bioquímica. Departamento de Ciencias Químicas. Universidad de Buenos Aires. Buenos Aires, Argentina. Instituto de Química y Metabolismo del Fármaco (IQUIMEFA). CONICET - Universidad de Buenos Aires. Buenos Aires, Argentina. Orcid: https://orcid.org/0000-0003-1878-1776, e-mail: dimaciodimacio@gmail.com.

Maibelin Rosales – Advanced Mining Technology Center (AMTC), Universidad de Chile, Beauchef 850, Santiago, Chile. Orcid: https://orcid.org/0000-0002-1972-7352, e-mail: maibelin.rosales@amtc.cl

Arkaitz Fidalgo-Marijuan – BCMaterials (Basque Center for Materials, Applications & Nanostructures), Bldg. Martina Casiano, 3rd. Floor, Barrio Sarriena s/n, 48940, Leioa, Spain. Orcid: https://orcid.org/0000-0001-7019-7249, e-mail: arkaitz.fidalgo@bcmaterials.net

José María Porro – BCMaterials (Basque Center for Materials, Applications & Nanostructures), Bldg. Martina Casiano, 3rd. Floor, Barrio Sarriena s/n, 48940, Leioa, Spain. IKERBASQUE, Basque Foundation for Science, 48009 Bilbao, Spain Orcid: https://orcid.org/0000-0002-8610-9802, e-mail: jm.porro@bcmaterials.net

Mónica Jiménez-Ruiz – Institut Laue Langevin, 71 Avenue des Martyrs, CS 20156, 38042 Grenoble, France. Orcid: https://orcid.org/0000-0002-9856-807X, e-mail: jimenez@ill.fr

Victoria Garcia Sakai – ISIS Neutron and Muon Facility, Science & Technology Facilities Council, Rutherford Appleton Laboratory, Didcot, United Kingdom. Orcid: https://orcid.org/0000-0001-6570-4218 , e-mail: victoria.garcia-sakai@stfc.ac.uk

Andreina García – Advanced Mining Technology Center (AMTC), Universidad de Chile, Beauchef 850, Santiago, Chile. Mining Engineering Department, FCFM, Universidad de Chile,

Av. Tupper 2069, 8370451 Santiago, Chile. Orcid: https://orcid.org/0000-0003-1607-8913, e-mail: andreina.garcia@amtc.cl.

José Manuel Laza– Macromolecular Chemistry Group (LABQUIMAC), Department of Physical Chemistry, Faculty of Science and Technology, University of the Basque Country (UPV/EHU), Barrio Sarriena s/n 48940 Leioa (Spain). Orcid: https://orcid.org/0000-0003-0412-621X, e-mail: josemanuel.laza@ehu.eus

José Luis Vilas-Vilela – BCMaterials (Basque Center for Materials, Applications & Nanostructures), Bldg. Martina Casiano, 3rd. Floor, Barrio Sarriena s/n, 48940, Leioa, Spain. Macromolecular Chemistry Group (LABQUIMAC), Department of Physical Chemistry, Faculty of Science and Technology, University of the Basque Country (UPV/EHU), Barrio Sarriena s/n 48940 Leioa (Spain). Orcid: https://orcid.org/0000-0002-0188-4579, e-mail: joseluis.vilas@ehu.eus

María I. Arriortua – Dept. of Geology, Science and Technology Faculty, University of the Basque Country (UPV/EHU), Barrio Sarriena s/n 48940 Leioa (Spain). Orcid: https://orcid.org/0000-0001-7562-2478, e-mail: maribel.arriortua@ehu.eus

Luis Lezama – Dept. of Inorganic Chemistry, Science and Technology Faculty, University of the Basque Country (UPV/EHU), Barrio Sarriena s/n 48940 Leioa (Spain). Orcid: https://orcid.org/0000-0001-6183-2052, e-mail: luis.lezama@ehu.eus

Guillermo Copello – Facultad de Farmacia y Bioquímica. Departamento de Ciencias Químicas. Universidad de Buenos Aires. Buenos Aires, Argentina. Instituto de Química y Metabolismo del

Fármaco (IQUIMEFA). CONICET - Universidad de Buenos Aires. Buenos Aires, Argentina. Orcid: https://orcid.org/0000-0003-2689-8202, e-mail: gcopello@ffyb.uba.ar

Author Contributions

The manuscript was written through contributions of all authors. All authors have given approval to the final version of the manuscript.

Notes

The authors declare no competing financial interest.

ACKNOWLEDGMENT

The authors thank financial support from the Spanish Agencia Estatal de Investigación (AEI) through EVOLMOF PID2021-122940OB-C31 (AEI/FEDER, UE) (including FEDER financial support), and Tailing43Green-ERAMIN projects. Basque Government Industry and Education Departments under the ELKARTEK, HAZITEK and PIBA (PIBA-2022-1-0032) programs, are also acknowledged. Ainara Valverde thanks the Basque Government (Education Department) for her PhD grant (PREB_2018_1_004). The MSCA-RISE-2017 (No 778412) INDESMOF, and H2020-RIA-4AirCraft (No 101022633) projects, which received funding from the European Union's Horizon 2020 research and innovation programme are also acknowledged. The authors thank the technical and human support provided by SGIker (UPV/EHU).

REFERENCES

(1) Tchounwou, P. B.; Yedjou, C. G.; Patlolla, A. K.; Sutton, D. J. Heavy Metal Toxicity and the Environment. In *Molecular, Clinical and Environmental Toxicology*; 2012; pp 133–164. https://doi.org/10.1007/978-3-7643-8340-4.

(2) G. Saiz, P.; Valverde, A.; Gonzalez-Navarrete, B.; Rosales, M.; Quintero, Y. M.; Fidalgo-Marijuan, A.; Orive, J.; Reizabal, A.; Larrea, E. S.; Arriortua, M. I.; Lanceros-Méndez, S.; García, A.; Fernández de Luis, R. Modulation of the Bifunctional CrVI to CrIII Photoreduction and Adsorption Capacity in ZrIV and TiIV Benchmark Metal-Organic Frameworks. *Catalysts*. 2021, pp 51–60. https://doi.org/10.3390/catal11010051.

(3) Naidu, G.; Ryu, S.; Thiruvenkatachari, R.; Choi, Y.; Jeong, S.; Vigneswaran, S. A Critical Review on Remediation, Reuse, and Resource Recovery from Acid Mine Drainage. *Environmental Pollution* **2019**, *247*, 1110–1124. https://doi.org/10.1016/j.envpol.2019.01.085.

(4) León, R.; Macías, F.; R. Cánovas, C.; Pérez-López, R.; Ayora, C.; Nieto, J. M.; Olías, M. Mine Waters as a Secondary Source of Rare Earth Elements Worldwide: The Case of the Iberian Pyrite Belt. *Journal of Geochemical Exploration* **2021**, *224* (September 2020). https://doi.org/10.1016/j.gexplo.2021.106742.

(5) Peng, Y.; Huang, H.; Liu, D.; Zhong, C. Radioactive Barium Ion Trap Based on Metal-Organic Framework for Efficient and Irreversible Removal of Barium from Nuclear Wastewater. *ACS Applied Materials and Interfaces* **2016**, *8* (13), 8527–8535. https://doi.org/10.1021/acsami.6b00900.

(6) Lin, S.; Zhao, Y.; Bediako, J. K.; Cho, C.; Sarkar, A. K.; Lim, C.; Yun, Y. Structure-Controlled Recovery of Palladium (II) from Acidic Aqueous Solution Using Metal-Organic Frameworks of MOF-802 , UiO-66 and MOF-808. *Chemical Engineering Journal* **2019**, No. Ii. https://doi.org/10.1016/j.cej.2019.01.044.

(7) Zha, M.; Liu, J.; Wong, Y. L.; Xu, Z. Extraction of Palladium from Nuclear Waste-like Acidic Solutions by a Metal-Organic Framework with Sulfur and Alkene Functions. *Journal of Materials Chemistry A* **2015**, *3* (7), 3928–3934. https://doi.org/10.1039/c4ta06678b.

(8) Sun, D. T.; Gasilova, N.; Yang, S.; Oveisi, E.; Queen, W. L. Rapid, Selective Extraction of Trace Amounts of Gold from Complex Water Mixtures with a Metal-Organic Framework (MOF)/Polymer Composite. *J Am Chem Soc* **2018**, *140* (48), 16697–16703. https://doi.org/10.1021/jacs.8b09555.

(9) Dinu, M. V.; Dragan, E. S. Heavy Metals Adsorption on Some Iminodiacetate Chelating Resins as a Function of the Adsorption Parameters. *Reactive and Functional Polymers* **2008**, *68* (9), 1346–1354. https://doi.org/10.1016/j.reactfunctpolym.2008.06.011.

(10) Henry, W. D.; Zhao, D.; SenGupta, A. K.; Lange, C. Preparation and Characterization of a New Class of Polymeric Ligand Exchangers for Selective Removal of Trace Contaminants from Water. *Reactive and Functional Polymers* **2004**, *60* (1–3), 109–120. https://doi.org/10.1016/j.reactfunctpolym.2004.02.016.

(11) Baraka, A.; Hall, P. J.; Heslop, M. J. Preparation and Characterization of Melamine-Formaldehyde-DTPA Chelating Resin and Its Use as an Adsorbent for Heavy Metals Removal from Wastewater. *Reactive and Functional Polymers* **2007**, *67* (7), 585–600. https://doi.org/10.1016/j.reactfunctpolym.2007.01.015.

(12) Chen, Y.; Tang, J.; Wang, S.; Zhang, L. Facile Preparation of a Remarkable MOF Adsorbent for Au(III) Selective Separation from Wastewater: Adsorption, Regeneration and Mechanism. *Journal of Molecular Liquids* **2022**, *349*, 118137. https://doi.org/10.1016/j.molliq.2021.118137.

(13) Tang, J.; Zhao, J.; Wang, S.; Zhang, L.; Zhao, M.; Huang, Z.; Hu, Y. Pre-Modification Strategy to Prepare a Novel Zr-Based MOF for Selective Adsorption of Palladium(II) from Solution. *Chemical Engineering Journal* **2021**, *407* (September 2020), 127223. https://doi.org/10.1016/j.cej.2020.127223.

(14) Peng, Y.; Huang, H.; Zhang, Y.; Kang, C.; Chen, S.; Song, L.; Liu, D.; Zhong, C. A Versatile MOF-Based Trap for Heavy Metal Ion Capture and Dispersion. *Nature Communications* **2018**, *9* (1). https://doi.org/10.1038/s41467-017-02600-2.

(15) Lu, X.; Wang, F.; Li, X.; Shih, K.; Zeng, E. Y. Adsorption and Thermal Stabilization of Pb 2+ and Cu 2+ by Zeolite. *Industrial & Engineering Chemistry Research* **2016**, *55*, 8767–8773. https://doi.org/10.1021/acs.iecr.6b00896.

(16) Seliman, A. F.; Lasheen, Y. F.; Youssief, M. A. E.; Shehata, F. A. Removal of Some Radionuclides from Contaminated Solution Using Natural Clay: Bentonite. *Journal of Radioanalytical and Nuclear Chemistry* **2014**, *300*, 969–979. https://doi.org/10.1007/s10967-014-3027-z.

(17) Krukowska, J.; Thomas, P.; Kołodyn, D. Comparison of Sorption and Desorption Studies of Heavy Metal Ions from Biochar and Commercial Active Carbon. *Chemical Engeneering Journal* **2017**, *307*, 353–363. https://doi.org/10.1016/j.cej.2016.08.088.

(18) Li, J.; Wang, X.; Power, E.; Zhao, G.; Chai, Z.; Chen, C.; Alsaedi, A.; Hayat, T.; Wang, X. Metal–Organic Framework-Based Materials: Superior Adsorbents for the Capture of Toxic and Radioactive Metal Ions. *Chemical Society Reviews* **2018**, *47*, 2322. https://doi.org/10.1039/c7cs00543a.

(19) Baek, J.; Rungtaweevoranit, B.; Pei, X.; Park, M.; Fakra, S. C.; Liu, Y. S.; Matheu, R.; Alshmimri, S. A.; Alshehri, S.; Trickett, C. A.; Somorjai, G. A.; Yaghi, O. M. Bioinspired Metal-Organic Framework Catalysts for Selective Methane Oxidation to Methanol. *J Am Chem Soc* **2018**, *140* (51), 18208–18216. https://doi.org/10.1021/jacs.8b11525.

(20) Ding, C.-W.; Luo, W.; Zhou, J.-Y.; Ma, X.-J.; Chen, G.-H.; Zhou, X.-P.; Li, D. Hydroxo Iron(III) Sites in a Metal–Organic Framework: Proton-Coupled Electron Transfer and Catalytic Oxidation of Alcohol with Molecular Oxygen. *ACS Applied Materials & Interfaces* **2019**, *11* (49), 45621–45628. https://doi.org/10.1021/acsami.9b15311.

(21) Sun, Q.; Aguila, B.; Ma, S. Metalloenzyme Mimicry at the Nodes of Metal-Organic Frameworks. *Chem* **2018**, *4* (12), 2736–2738. https://doi.org/10.1016/j.chempr.2018.11.017.

(22) Chiong, J. A.; Zhu, J.; Bailey, J. B.; Kalaj, M.; Subramanian, R. H.; Xu, W.; Cohen, S. M.; Tezcan, F. A. An Exceptionally Stable Metal-Organic Framework Constructed from Chelate-Based Metal-Organic Polyhedra. *J Am Chem Soc* **2020**, *142* (15), 6907–6912. https://doi.org/10.1021/jacs.0c01626.

(23) Ji, Z.; Wang, H.; Canossa, S.; Wuttke, S.; Yaghi, O. M. Pore Chemistry of Metal–Organic Frameworks. *Advanced Functional Materials* **2020**, *30* (41), 2000238. https://doi.org/https://doi.org/10.1002/adfm.202000238.

(24) Gropp, C.; Canossa, S.; Wuttke, S.; Gándara, F.; Li, Q.; Gagliardi, L.; Yaghi, O. M. Standard Practices of Reticular Chemistry. *ACS Central Science* **2020**, *6* (8), 1255–1273. https://doi.org/10.1021/acscentsci.0c00592.

(25) Larrea, E. S.; Fernández De Luis, R.; Orive, J.; Iglesias, M.; Arriortua, M. I. Mixed Metal-Organic Framework as a Heterogeneous Catalyst. *European Journal of Inorganic Chemistry* **2015**, *2015* (28). https://doi.org/10.1002/ejic.201500431.

(26) Freund, R.; Canossa, S.; Cohen, S. M.; Yan, W.; Deng, H.; Guillerm, V.; Eddaoudi, M.; Madden, D. G.; Fairen-Jimenez, D.; Lyu, H.; Macreadie, L. K.; Ji, Z.; Zhang, Y.; Wang, B.; Haase, F.; Wöll, C.; Zaremba, O.; Andreo, J.; Wuttke, S.; Diercks, C. S. 25 Years of Reticular Chemistry. *Angewandte Chemie International Edition* **2021**, *60* (45), 23946–23974. https://doi.org/10.1002/anie.202101644.

(27) Valverde, A.; Gonçalves, R.; Silva, M. M.; Wuttke, S.; Fidalgo-Marijuan, A.; Costa, C. M.; Vilas-Vilela, J. L.; Laza, J. M.; Arriortua, M. I.; Lanceros-Méndez, S.; Fernández de Luis, R. Metal–Organic Framework Based PVDF Separators for High Rate Cycling Lithium-Ion Batteries. *ACS Applied Energy Materials* **2020**, *3* (12), 11907–11919. https://doi.org/10.3390/catal11010051.

(28) Assi, H.; Mouchaham, G.; Steunou, N.; Devic, T.; Serre, C. Titanium Coordination Compounds: From Discrete Metal Complexes to Metal-Organic Frameworks. *Chemical Society Reviews* **2017**, *46* (11), 3431–3452. https://doi.org/10.1039/c7cs00001d.

(29) Mouchaham, G.; Wang, S.; Serre, C. The Stability of Metal-Organic Frameworks. *Metal-Organic Frameworks* **2018**, No. i, 1–28. https://doi.org/10.1002/9783527809097.ch1.

(30) Lin, K. A.; Chen, S.; Jochems, A. P. Zirconium-Based Metal Organic Frameworks : Highly Selective Adsorbents for Removal of Phosphate from Water and Urine. *Materials Chemistry and Physics* **2015**, 1–9. https://doi.org/10.1016/j.matchemphys.2015.04.021.

(31) Freund, R.; Zaremba, O.; Arnauts, G.; Ameloot, R.; Skorupskii, G.; Dincă, M.; Bavykina, A.; Gascon, J.; Ejsmont, A.; Gościańska, J.; Kalmutzki, M.; Lächelt, U.; Ploetz, E.; Diercks, C.; Wuttke, S. The Current Status of MOF and COF Applications. *Angewandte Chemie International Edition* **2021**, *60* (45), 23975–24001. https://doi.org/10.1002/anie.202106259.

(32) Maleki, A.; Hayati, B.; Naghizadeh, M.; Joo, S. W. Adsorption of Hexavalent Chromium by Metal Organic Frameworks from Aqueous Solution. *Journal of Industrial and Engineering Chemistry* **2015**, *28*, 211–216. https://doi.org/10.1016/j.jiec.2015.02.016.

(33) Wang, C.; Liu, X.; Chen, J. P.; Li, K. Superior Removal of Arsenic from Water with Zirconium Metal-Organic Framework UiO-66. *Scientific Reports* **2015**, *5*, 1–10. https://doi.org/10.1038/srep16613.

(34) Howarth, A. J.; Katz, M. J.; Wang, T. C.; Platero-Prats, A. E.; Chapman, K. W.; Hupp, J. T.; Farha, O. K. High Efficiency Adsorption and Removal of Selenate and Selenite from Water Using Metal-Organic Frameworks. *J Am Chem Soc* **2015**, *137* (23), 7488–7494. https://doi.org/10.1021/jacs.5b03904.

(35) De Decker, J.; Rochette, J.; De Clercq, J.; Florek, J.; Van Der Voort, P. Carbamoylmethylphosphine Oxide-Functionalized MIL-101(Cr) as Highly Selective Uranium Adsorbent. *Analytical Chemistry* **2017**, *89* (11), 5678–5682. https://doi.org/10.1021/acs.analchem.7b00821.

(36) Healey, K.; Liang, W.; Southon, P. D.; Church, T. L.; D'Alessandro, D. M. Photoresponsive Spiropyran-Functionalised MOF-808: Postsynthetic Incorporation and Light Dependent Gas Adsorption Properties. *Journal of Materials Chemistry A* **2016**, *4* (28), 10816–10819. https://doi.org/10.1039/c6ta04160d.

(37) Karagiaridi, O.; Bury, W.; Mondloch, J. E.; Hupp, J. T.; Farha, O. K. Solvent-Assisted Linker Exchange: An Alternative to the de Novo Synthesis of Unattainable Metal-Organic Frameworks. *Angewandte Chemie - International Edition* **2014**, *53* (18), 4530–4540. https://doi.org/10.1002/anie.201306923.

(38) Deria, P.; Bury, W.; Hod, I.; Kung, C. W.; Karagiaridi, O.; Hupp, J. T.; Farha, O. K. MOF Functionalization via Solvent-Assisted Ligand Incorporation: Phosphonates vs Carboxylates. *Inorganic Chemistry* **2015**, *54* (5), 2185–2192. https://doi.org/10.1021/ic502639v.

(39) Kalaj, M.; Cohen, S. M. Postsynthetic Modification: An Enabling Technology for the Advancement of Metal-Organic Frameworks. *ACS Central Science* **2020**, *6* (7), 1046–1057. https://doi.org/10.1021/acscentsci.0c00690.

(40) al Danaf, N.; Schrimpf, W.; Hirschle, P.; Lamb, D. C.; Ji, Z.; Wuttke, S. Linker Exchange via Migration along the Backbone in Metal-Organic Frameworks. *J Am Chem Soc* **2021**, *143* (28), 10541–10546. https://doi.org/10.1021/jacs.1c04804.

(41) Mon, M.; Bruno, R.; Ferrando-Soria, J.; Armentano, D.; Pardo, E. Metal–Organic Framework Technologies for Water Remediation: Towards a Sustainable Ecosystem. *Journal of Materials Chemistry A* **2018**, *6* (12), 4912–4947. https://doi.org/10.1039/C8TA00264A.

(42) Reizabal, A.; Costa, C. M.; Saiz, P. G.; Gonzalez, B.; Pérez-Álvarez, L.; Fernández de Luis, R.; Garcia, A.; Vilas-Vilela, J. L.; Lanceros-Méndez, S. Processing Strategies to Obtain Highly Porous Silk Fibroin Structures with Tailored Microstructure and Molecular

Characteristics and Their Applicability in Water Remediation. *Journal of Hazardous Materials* **2021**, *403*, 123675. https://doi.org/https://doi.org/10.1016/j.jhazmat.2020.123675.

(43) Wang, K.; Gu, J.; Yin, N. Efficient Removal of Pb(II) and Cd(II) Using NH2-Functionalized Zr-MOFs via Rapid Microwave-Promoted Synthesis. *Industrial and Engineering Chemistry Research* **2017**, *56* (7), 1880–1887. https://doi.org/10.1021/acs.iecr.6b04997.

(44) Muguruza, A. R.; de Luis, R. F.; Iglesias, N.; Bazán, B.; Urtiaga, M. K.; Larrea, E. S.; Fidalgo-Marijuan, A.; Barandika, G. Encapsulation of β-Alanine Model Amino-Acid in Zirconium(IV) Metal Organic Frameworks: Defect Engineering to Improve Host Guest Interactions. *Journal of Inorganic Biochemistry* **2020**, *205* (July 2019), 110977. https://doi.org/10.1016/j.jinorgbio.2019.110977.

(45) Custelcean, R.; Moyer, B. A. Anion Separation with Metal – Organic Frameworks. *European Journal of Inorganic Chemistry* **2007**, *2007* (10), 1321–1340. https://doi.org/10.1002/ejic.200700018.

(46) Becker, F. G.; Cleary, M.; Team, R. M.; Holtermann, H.; The, D.; Agenda, N.; Science, P.; Sk, S. K.; Hinnebusch, R.; Hinnebusch A, R.; Rabinovich, I.; Olmert, Y.; Uld, D. Q. G. L. Q.; Ri, W. K. H. U.; Lq, V.; Frxqwu, W. K. H.; Zklfk, E.; Edvhg, L. V; Wkh, R. Q.; Becker, F. G.; Aboueldahab, N.; Khalaf, R.; De Elvira, L. R.; Zintl, T.; Hinnebusch, R.; Karimi, M.; Mousavi Shafaee, S. M.; O 'driscoll, D.; Watts, S.; Kavanagh, J.; Frederick, B.; Norlen, T.; O'Mahony, A.; Voorhies, P.; Szayna, T.; Spalding, N.; Jackson, M. O.; Morelli, M.; Satpathy, B.; Muniapan, B.; Dass, M.; Katsamunska, P.; Pamuk, Y.; Stahn, A.; Commission, E.; Piccone, T. E. D.; Annan, Mr. K.; Djankov, S.; Reynal-Querol, M.; Couttenier, M.; Soubeyran, R.; Vym, P.; Prague, E.; World Bank; Bodea, C.; Sambanis, N.; Florea, A.; Florea, A.; Karimi, M.; Mousavi Shafaee, S. M.; Spalding, N.; Sambanis, N.; فاطمی, ح. *Reviews of Environmental Contamination and Toxicology. Volume 196*; Whitacre, D. M., Ed.; Springer, 2015; Vol. 7.

(47) Azimi, A.; Azari, A.; Rezakazemi, M.; Ansarpour, M. Removal of Heavy Metals from Industrial Wastewaters: A Review. *ChemBioEng Reviews* **2017**, *4* (1), 37–59. https://doi.org/10.1002/cben.201600010.

(48) Jiang, J.; Gándara, F.; Zhang, Y. B.; Na, K.; Yaghi, O. M.; Klemperer, W. G. Superacidity in Sulfated Metal-Organic Framework-808. *J Am Chem Soc* **2014**, *136* (37), 12844–12847. https://doi.org/10.1021/ja507119n.

(49) Bernales, V.; Ortuño, M. A.; Truhlar, D. G.; Cramer, C. J.; Gagliardi, L. Computational Design of Functionalized Metal-Organic Framework Nodes for Catalysis. *ACS Central Science* **2018**, *4* (1), 5–19. https://doi.org/10.1021/acscentsci.7b00500.

(50) Ke, F.; Qiu, L. G.; Yuan, Y. P.; Peng, F. M.; Jiang, X.; Xie, A. J.; Shen, Y. H.; Zhu, J. F. Thiol-Functionalization of Metal-Organic Framework by a Facile Coordination-Based Postsynthetic Strategy and Enhanced Removal of Hg 2+ from Water. *Journal of Hazardous Materials* **2011**, *196*, 36–43. https://doi.org/10.1016/j.jhazmat.2011.08.069.

(51) Baumann, A. E.; Burns, D. A.; Liu, B.; Thoi, V. S. Metal-Organic Framework Functionalization and Design Strategies for Advanced Electrochemical Energy Storage Devices. *Communications Chemistry* **2019**, *2* (1), 1–14. https://doi.org/10.1038/s42004-019-0184-6.

(52) Rosales, M.; Orive, J.; Espinoza-González, R.; Fernández de Luis, R.; Gauvin, R.; Brodusch, N.; Rodríguez, B.; Gracia, F.; García, A. Evaluating the Bi-Functional Capacity for Arsenic Photo-Oxidation and Adsorption on Anatase TiO2 Nanostructures with Tunable Morphology. *Chemical Engineering Journal* **2021**, *415*, 128906. https://doi.org/https://doi.org/10.1016/j.cej.2021.128906.

(53) Tovar Jimenez, G. I.; Valverde, A.; Mendes-Felipe, C.; Wuttke, S.; Fidalgo-Marijuan, A.; Larrea, E. S.; Lezama, L.; Zheng, F.; Reguera, J.; Lanceros-Méndez, S.; Arriortua, M. I.; Copello, G.; de Luis, R. F. Chitin/Metal-Organic Framework Composites as Wide-Range Adsorbent. *ChemSusChem* **2021**, *n/a* (n/a). https://doi.org/https://doi.org/10.1002/cssc.202100675.

(54) Rapti, S.; Pournara, A.; Sarma, D.; Papadas, I. T.; Armatas, G. S.; Hassan, Y. S.; Alkordi, M. H.; Kanatzidis, M. G.; Manos, M. J. Rapid, Green and Inexpensive Synthesis of High Quality UiO-66 Amino-Functionalized Materials with Exceptional Capability for Removal of Hexavalent Chromium from Industrial Waste. *Inorganic Chemistry Frontiers* **2016**, *3* (5), 635–644. https://doi.org/10.1039/C5QI00303B.

(55) Allen, S. J.; Mckay, G.; Porter, J. F. Adsorption Isotherm Models for Basic Dye Adsorption by Peat in Single and Binary Component Systems. *Journal of Colloid and Interface Science* **2004**, *280* (2), 322–333. https://doi.org/10.1016/j.jcis.2004.08.078.

(56) Valverde, A.; G.-Sainz, P.; Orive, J.; E., L.; Reizabal-Para, A.; Tovar, G.; Copello, G.; Lazaro-Martinez, J. M.; Rodriguez, B.; Gonzalez-Navarrete, B.; Quintero, M. Y.; Rosales, M.; García, A.; Arriortua, M. I.; Fernandez de Luis, R. Porous, Lightweight, Metal Organic Materials: Environment Sustainability. In *Advanced Lightweight Multifunctional Materials*; Elsevier, 2020; pp 43–130.

(57) Peralta Ramos, M. L.; González, J. A.; Albornoz, S. G.; Pérez, C. J.; Villanueva, M. E.; Giorgieri, S. A.; Copello, G. J. Chitin Hydrogel Reinforced with TiO2 Nanoparticles as an Arsenic Sorbent. *Chemical Engineering Journal* **2016**, *285*, 581–587. https://doi.org/10.1016/j.cej.2015.10.035.

(58) Gil, A.; Assis, F. C. C.; Albeniz, S.; Korili, S. A. Removal of Dyes from Wastewaters by Adsorption on Pillared Clays. *Chemical Engineering Journal* **2011**, *168* (3), 1032–1040. https://doi.org/10.1016/j.cej.2011.01.078.

(59) Zhang, W.; Bu, A.; Ji, Q.; Min, L.; Zhao, S.; Wang, Y.; Chen, J. PKa-Directed Incorporation of Phosphonates into Mof-808 via Ligand Exchange: Stability and Adsorption Properties for Uranium. *ACS Applied Materials and Interfaces* **2019**, *11* (37), 33931–33940. https://doi.org/10.1021/acsami.9b10920.

(60) Du, Y.; Fang, H. X.; Zhang, Q.; Zhang, H. L.; Hong, Z. Spectroscopic Investigation on Cocrystal Formation between Adenine and Fumaric Acid Based on Infrared and Raman

Techniques. *Spectrochimica Acta - Part A: Molecular and Biomolecular Spectroscopy* **2016**, *153*, 580–585. https://doi.org/10.1016/j.saa.2015.09.020.

(61) Mesu, J. G.; Visser, T.; Soulimani, F.; Weckhuysen, B. M. Infrared and Raman Spectroscopic Study of PH-Induced Structural Changes of L-Histidine in Aqueous Environment. *Vib Spectrosc* **2005**, *39* (1), 114–125. https://doi.org/10.1016/j.vibspec.2005.01.003.

(62) Hargreaves, M. K.; Stevinson, E. A. The Infra-Red Spectra of Fumaramic and Maleamic Acids and Their Sodium Salts. *Spectrochimica Acta* **1965**, *21* (9), 1681–1689. https://doi.org/10.1016/0371-1951(65)80079-0.

(63) Shearer, G. C.; Chavan, S.; Ethiraj, J.; Vitillo, J. G.; Svelle, S.; Olsbye, U.; Lamberti, C.; Bordiga, S.; Lillerud, K. P. Tuned to Perfection: Ironing out the Defects in Metal-Organic Framework UiO-66. *Chemistry of Materials* **2014**, *26* (14), 4068–4071. https://doi.org/10.1021/cm501859p.

(64) Hardian, R.; Dissegna, S.; Ullrich, A.; Llewellyn, P. L.; Coulet, M. V.; Fischer, R. A. Tuning the Properties of MOF-808 via Defect Engineering and Metal Nanoparticle Encapsulation. *Chemistry - A European Journal* **2021**, *27* (22), 6804–6814. https://doi.org/10.1002/chem.202005050.

(65) Basu, O.; Mukhopadhyay, S.; Laha, S.; Das, S. K. Defect Engineering in a Metal − Organic Framework System to Achieve Super-Protonic Conductivity. *Chemistry of Materials* **2022**, *XXX*, XXX–XXX. https://doi.org/10.1021/acs.chemmater.2c00654.

(66) Ardila-Suárez, C.; Perez-Beltran, S.; Ramírez-Caballero, G. E.; Balbuena, P. B. Enhanced Acidity of Defective MOF-808: Effects of the Activation Process and Missing Linker Defects. *Catalysis Science and Technology* **2018**, *8* (3), 847–857. https://doi.org/10.1039/c7cy02462b.

(67) Lyu, H.; Chen, O. I. F.; Hanikel, N.; Hossain, M. I.; Flaig, R. W.; Pei, X.; Amin, A.; Doherty, M. D.; Impastato, R. K.; Glover, T. G.; Moore, D. R.; Yaghi, O. M. Carbon Dioxide Capture Chemistry of Amino Acid Functionalized Metal-Organic Frameworks in Humid Flue Gas. *J Am Chem Soc* **2022**, *144* (5), 2387–2396. https://doi.org/10.1021/jacs.1c13368.

(68) Furukawa, H.; Gándara, F.; Zhang, Y. B.; Jiang, J.; Queen, W. L.; Hudson, M. R.; Yaghi, O. M. Water Adsorption in Porous Metal-Organic Frameworks and Related Materials. *J Am Chem Soc* **2014**, *136* (11), 4369–4381. https://doi.org/10.1021/ja500330a.

(69) Wu, J.; Zhou, J.; Zhang, S.; Alsaedi, A.; Hayat, T.; Li, J.; Song, Y. Efficient Removal of Metal Contaminants by EDTA Modified MOF from Aqueous Solutions. *Journal of Colloid and Interface Science* **2019**, *555*, 403–412. https://doi.org/10.1016/j.jcis.2019.07.108.

(70) Saiz, P. G.; Iglesias, N.; González Navarrete, B.; Rosales, M.; Quintero, Y. M.; Reizabal, A.; Orive, J.; Fidalgo Marijuan, A.; Larrea, E. S.; Lopes, A. C.; Lezama, L.; García, A.; Lanceros-Mendez, S.; Arriortua, M. I.; Fernández de Luis, R. Chromium Speciation in Zirconium-Based Metal–Organic Frameworks for Environmental Remediation. *Chemistry*

- *A European Journal* **2020**, *26* (61), 13861–13872. https://doi.org/10.1002/chem.202001435.

(71) Li, Z.; Peters, A. W.; Bernales, V.; Ortuño, M. A.; Schweitzer, N. M.; Destefano, M. R.; Gallington, L. C.; Platero-Prats, A. E.; Chapman, K. W.; Cramer, C. J.; Gagliardi, L.; Hupp, J. T.; Farha, O. K. Metal-Organic Framework Supported Cobalt Catalysts for the Oxidative Dehydrogenation of Propane at Low Temperature. *ACS Central Science* **2017**, *3* (1), 31–38. https://doi.org/10.1021/acscentsci.6b00290.

(72) Pearson, R. G. Hard and Soft Acids and Bases. *J Am Chem Soc* **1963**, *85* (22), 3533–3539.

(73) Ifthikar, J.; Zhao, M.; Shahzad, A.; Shahib, I. I.; Wang, J.; Wang, H.; Sellaoui, L.; Chen, Z.; Chen, Z. Recyclable Process Modeling Study of Hexavalent Chromium Elimination by Thiol-Based Electron Donor: Implications for Practical Applicability. *Journal of Environmental Chemical Engineering* **2021**, *9* (4), 105645. https://doi.org/10.1016/j.jece.2021.105645.

(74) Kinuthia, G. K.; Ngure, V.; Beti, D.; Lugalia, R.; Wangila, A.; Kamau, L. Levels of Heavy Metals in Wastewater and Soil Samples from Open Drainage Channels in Nairobi, Kenya: Community Health Implication. *Scientific Reports* **2020**, *10* (1), 1–13. https://doi.org/10.1038/s41598-020-65359-5.

(75) Mon, M.; Lloret, F.; Ferrando-Soria, J.; Marta-Gastaldo, C.; Armentano, D.; Pardo, E. Selective and Efficient Removal of Mercury from Aqueous Media with the Highly Flexible Arms of a BioMOF. *Angewandte Chemie - International Edition* **2016**, *55* (37), 11167–11172. https://doi.org/10.1002/anie.201606015.

(76) Gala, L.; Lawson, M.; Jomova, K.; Zelenicky, L.; Congradyova, A.; Mazur, M.; Valko, M. EPR Spectroscopy of a Clinically Active (1:2) Copper(II)-Histidine Complex Used in the Treatment of Menkes Disease: A Fourier Transform Analysis of a Fluid CW-EPR Spectrum. *Molecules* . 2014. https://doi.org/10.3390/molecules19010980.

(77) Krupa, K.; Korabik, M.; Kowalik-Jankowska, T. Coordination Properties of Cu(II) Ions towards the Peptides Based on the His-Xaa-His Motif from Fusobacterium Nucleatum P1 Protein. *Journal of Inorganic Biochemistry* **2019**, *201*, 110819. https://doi.org/https://doi.org/10.1016/j.jinorgbio.2019.110819.

(78) Holm, R. H.; Kennepohl, P.; Solomon, E. I. Structural and Functional Aspects of Metal Sites in Biology. *Chemical Reviews* **1996**, *96* (7), 2239–2314. https://doi.org/10.1021/cr9500390.

(79) Maiti, B. K.; Maia, L. B.; Moro, A. J.; Lima, J. C.; Cordas, C. M.; Moura, I.; Moura, J. J. G. Unusual Reduction Mechanism of Copper in Cysteine-Rich Environment. *Inorganic Chemistry* **2018**, *57* (14), 8078–8088. https://doi.org/10.1021/acs.inorgchem.8b00121.

(80) Bennett, B.; Kowalski, J. M. Chapter Thirteen - EPR Methods for Biological Cu(II): L-Band CW and NARS. In *Electron Paramagnetic Resonance Investigations of Biological Systems by Using Spin Labels, Spin Probes, and Intrinsic Metal Ions, Part A*; Qin, P. Z.,

Warncke, K. B. T.-M. in E., Eds.; Academic Press, 2015; Vol. 563, pp 341–361. https://doi.org/https://doi.org/10.1016/bs.mie.2015.06.030.

(81) Parker, S. F. Assignment of the Vibrational Spectrum of L-Cysteine. *Chemical Physics* **2013**, *424*, 75–79. https://doi.org/10.1016/j.chemphys.2013.04.020.

(82) Dokken, K. M.; Parsons, J. G.; McClure, J.; Gardea-Torresdey, J. L. Synthesis and Structural Analysis of Copper(II) Cysteine Complexes. *Inorganica Chimica Acta* **2009**, *362* (2), 395–401. https://doi.org/10.1016/j.ica.2008.04.037.

SYNOPSIS

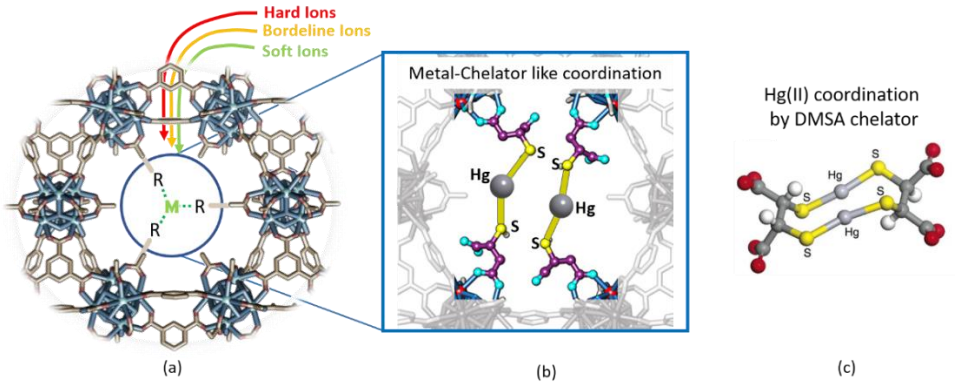

We have installed amino acid-type functionalities within porous space of MOF-808 tuning its adsorption capacity to capture metal ions of different acidities. Once the (amino)acids are installed in the framework, they resemble the multidentate metal coordination functions shown by organic chelator molecules.